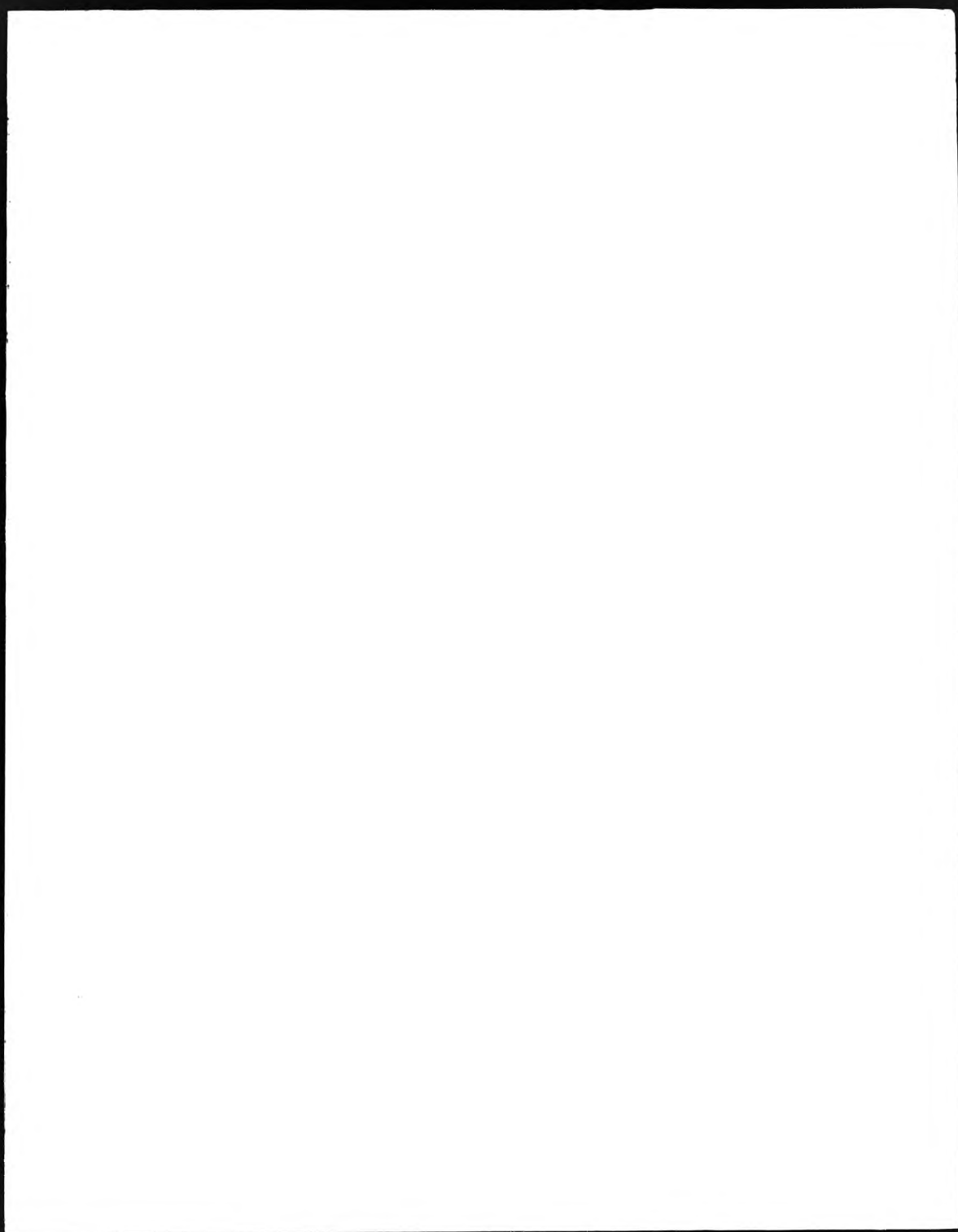
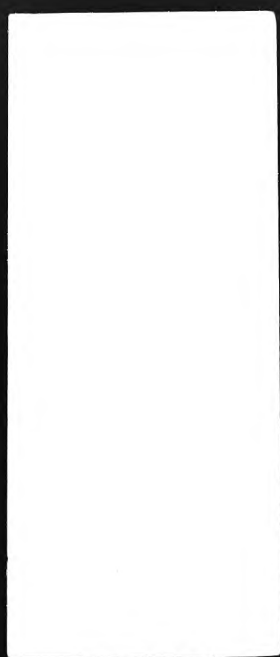
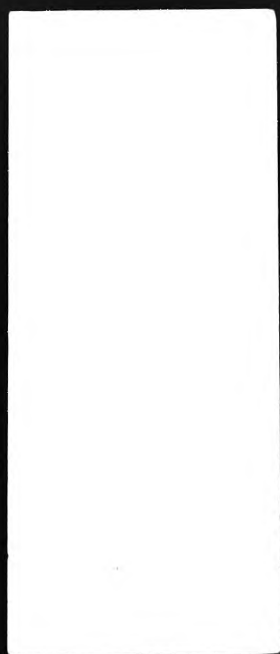


This PDF was created from the British Library's microfilm copy of the original thesis. As such the images are greyscale and no colour was captured.

Due to the scanning process, an area greater than the page area is recorded and extraneous details can be captured.

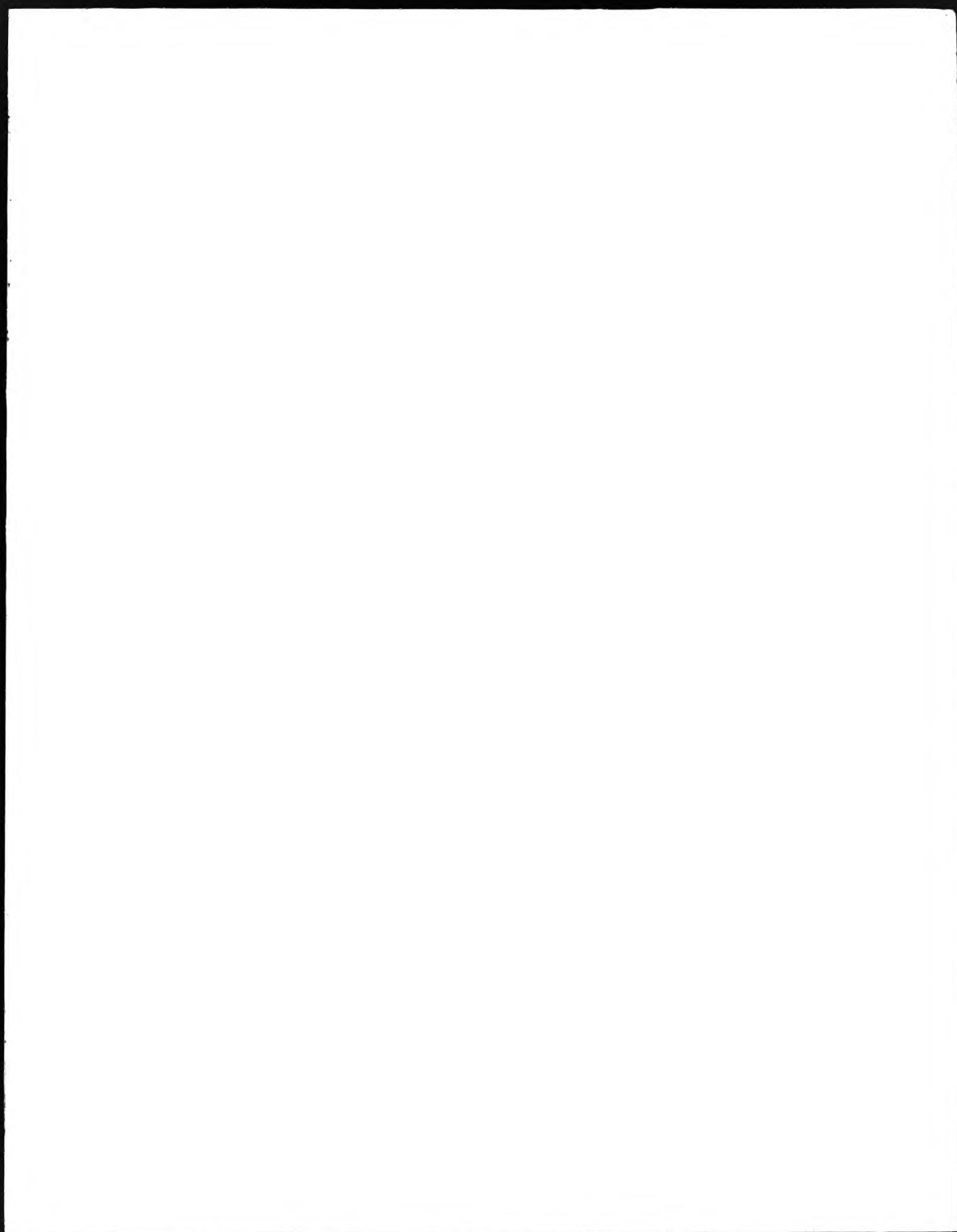
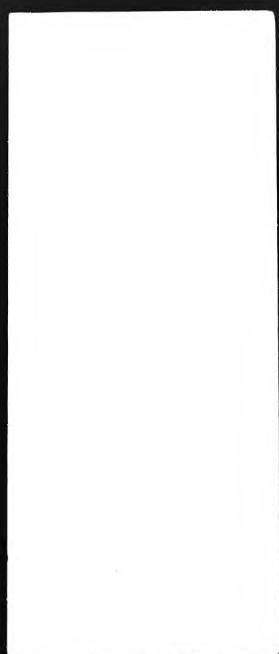
This is the best available copy





DX

9 4 4 6 3



THE BRITISH LIBRARY DOCUMENT SUPPLY CENTRE

TITLE

THE EFFECT OF MANGANESE AND NICKEL ON THE CLEAVAGE FRACTURE

STRENGTH OF FERRITIC WELD METAL

AUTHOR

Andrew Robert Brian Sandford

**INSTITUTION
and DATE**

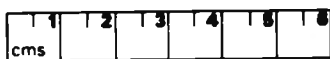
City of London Polytechnic 1990

CHAA

Attention is drawn to the fact that the copyright of this thesis rests with its author.

This copy of the thesis has been supplied on condition that anyone who consults it is understood to recognise that its copyright rests with its author and that no information derived from it may be published without the author's prior written consent.

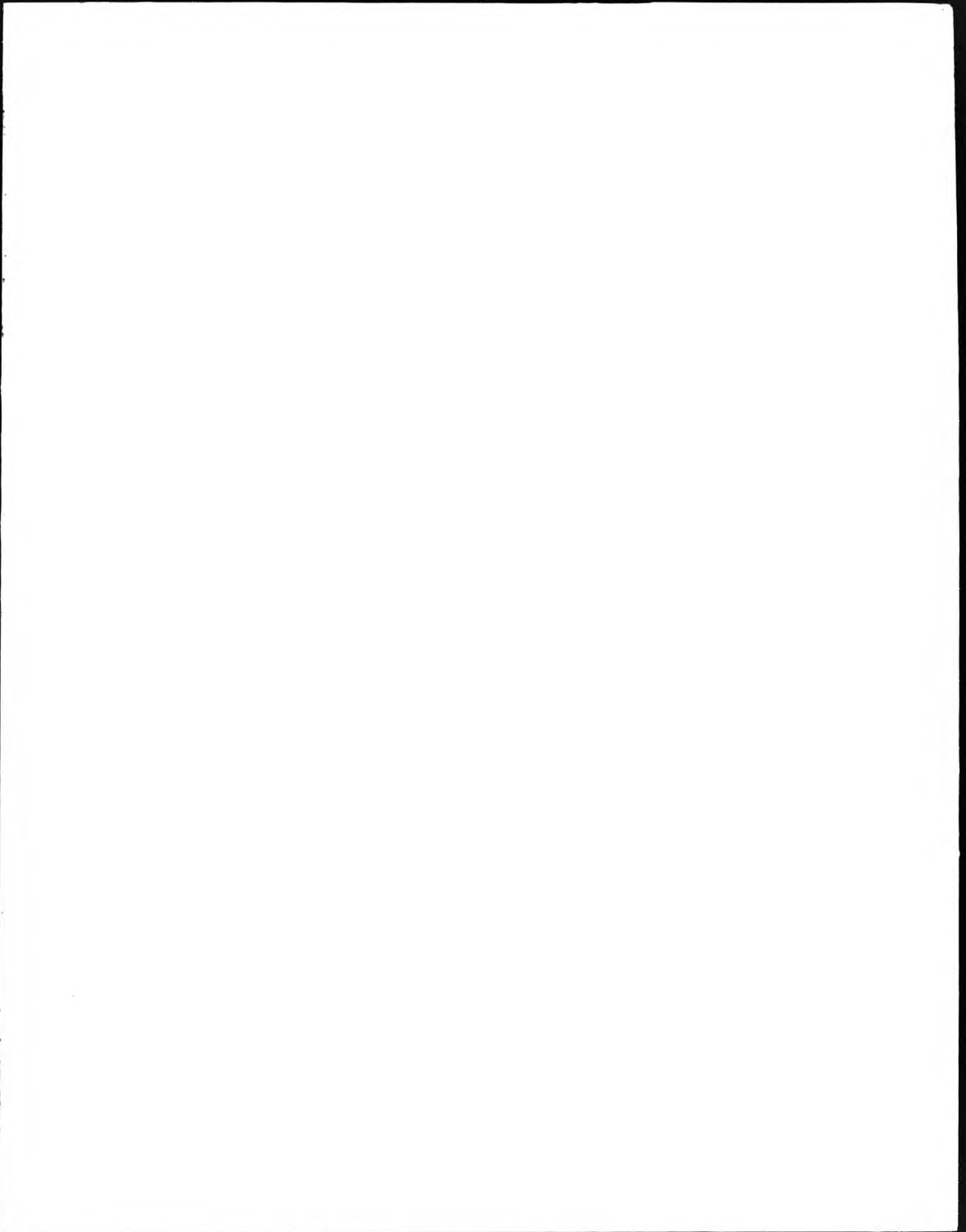
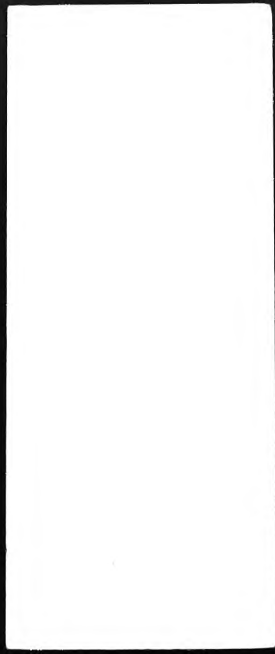
THE BRITISH LIBRARY
DOCUMENT SUPPLY CENTRE
Boston Spa, Wetherby
West Yorkshire
United Kingdom



20

REDUCTION X

5



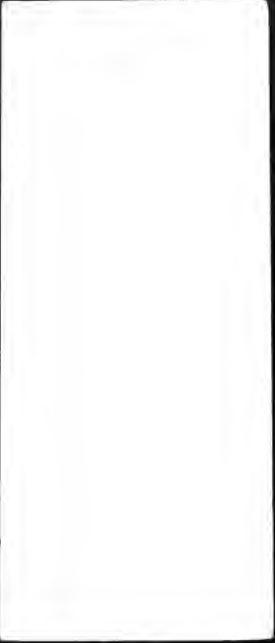
THE EFFECT OF MANGANESE AND NICKEL ON THE CLEAVAGE FRACTURE
STRENGTH OF FERRITIC WELD METAL

By Andrew Robert Brian Sandford BSc Hons

Submitted for the qualification of PhD in partial fulfilment of
the requirements of the CNAA in October 1990

This research was conducted at the City of London Polytechnic
in collaboration with Murex Welding Products Ltd

(Part of the ESAB Group)



THE BRITISH LIBRARY DOCUMENT SUPPLY CENTRE

BRITISH THESES NOTICE

The quality of this reproduction is heavily dependent upon the quality of the original thesis submitted for microfilming. Every effort has been made to ensure the highest quality of reproduction possible.

If pages are missing, contact the university which granted the degree.

Some pages may have indistinct print, especially if the original pages were poorly produced or if the university sent us an inferior copy.

Previously copyrighted materials (journal articles, published texts, etc.) are not filmed.

Reproduction of this thesis, other than as permitted under the United Kingdom Copyright Designs and Patents Act 1988, or under specific agreement with the copyright holder, is prohibited.

THIS THESIS HAS BEEN MICROFILMED EXACTLY AS RECEIVED

**THE BRITISH LIBRARY
DOCUMENT SUPPLY CENTRE
Boston Spa, Wetherby
West Yorkshire, LS23 7BQ
United Kingdom**

The author would like to acknowledge the support of Murex Welding Products for this research and thank the following people for their contributions without which this thesis would not have been possible:

Firstly my supervisor Dr Ray Jarman who provided a model that all supervisors would do well to emulate; my former colleagues at the sadly defunct Metallurgy Department of the City of London Polytechnic; my friends for their moral support and in particular Dee Barton for also adding actual support by typing large sections of the manuscript; and finally though by no means least my parents and fiancée Carol who offered continuous encouragement even when they received little thanks in return.

CONTENTS	PAGE
ABSTRACT	001
1. INTRODUCTION	002
2. LITERATURE REVIEW	007
2.1 Introduction	007
2.2 Welding metallurgy and the influence of alloying additions	018
2.2.1 The influence of alloying additions on weld metal microstructure	019
2.2.2 The effect of alloying on weld metal toughness	022
2.2.3 Strengthening mechanisms	023
2.2.4 Toughness of ferritic weld metal	026
2.3 Approaches to toughness characterisation	032
2.3.1 The Charpy V notch method	032
2.3.2 Plane strain fracture toughness	037
2.4 Cleavage fracture of ferritic weld metal	040
3. EXPERIMENTAL METHODS	048
3.1 Introduction	048
3.2 Experimental materials	049
3.3 Welding procedure	050
3.4 Test piece preparation	052
3.5 Homogenisation of microstructure	053
3.6 Cryostatic test cell	055
3.6.1 General requirements	055
3.6.2 Inner chamber	055
3.6.3 Outer chamber	056

3.6.4 Liquid nitrogen pump	057
3.7 Mechanical test procedure for cleavage fracture stress determination	058
3.7.1 Temperature rise during testing	058
3.7.2 Strain measurement	059
3.7.3 Load measurement	059
3.7.4 Cleavage fracture stress calculation	060
3.7.5 General yield load determination	061
3.7.6 Specimen preservation	061
3.8 Plane strain fracture toughness testing (K_{IC})	062
3.8.1 Fatigue pre-cracking	062
3.8.2 Determination of K_Q	066
3.9 Tensile testing	067
3.10 Impact testing of weld metal samples	068
3.11 Electron microscopy	069
3.12 Optical microscopy	069
3.13 Chemical analysis	069
4. EXPERIMENTAL RESULTS	070
4.1 Consistency of welds	070
4.2 Consistency of heat treatment	070
4.3 Microstructure and grain size of re-heated weld metal	071
4.4 Chemical analysis	073
4.5 Mechanical testing	074
4.5.1 Notched bend testing of as-welded samples	074
4.5.2 Notched bend testing of heat treated samples	076
4.5.2.1 7016 and 7016C1	076

4.5.2.2 Experimental electrodes A,C,D,E,F,G	078
4.5.2.3 Comparison of general yield loads for re-heated material	081
4.5.2.4 Comparison of fracture loads for re-heated material	082
4.5.2.5 Comparison of cleavage fracture strength	083
4.5.2.6 Effect of alloying additions on temperature at which coincidence of fracture and general yielding occurred	087
4.5.3 Plane strain fracture toughness testing of re-heated samples	088
4.6 Electron microscopy	091
4.6.1 Comparison of fracture surfaces for as-welded 7016 and 7016C1	
4.6.2 Comparison of as-welded and re-heated 7016 and 7016C1 fracture surfaces	093
4.6.3 Fracture surfaces of re-heated experimental electrodes	094
5.DISCUSSION AND CONCLUSIONS	096
5.1 Grain size effects and general yielding	096
5.2 The effects of alloying on grain size	099
5.3 Lüders strain	103
5.4 Differences between general yielding of as-welded material and re-heated material	105
5.5 Effect of alloying on general yield strength	106
5.6 Effects of alloying on cleavage fracture strength	107

5.7 Correlation between K_{IC} and cleavage fracture strength	115
5.8 Conclusion and suggestions for further research	117

FIGURES	PAGE
Fig(3.3.1) The position and sequence of welding runs and test plate clamping arrangement.	120
Fig(3.4.1) Test piece geometry	120
Fig(3.6.1) Cryostatic test cell	121
Fig(3.7.5.1) Geometric construction to obtain general yield load	122
Fig(3.8.1.1) Limiting envelope in which the fatigue pre- crack for K_{IC} test-piece must fall	122
Fig(4.2.1) Typical cooling curves after heat treatment (example shown is for composition A)	123
Fig(4.3.1) Photo-micrograph of re-heated microstructure 7016 (x 150)	124
Fig(4.3.2) Photo-micrograph of re-heated microstructure 7016C1 (x 150)	124
Fig(4.3.3) Photo-micrograph of re-heated microstructure A (x 150)	125
Fig(4.3.4) Photo-micrograph of re-heated microstructure C (x 150)	125
Fig(4.3.5) Photo-micrograph of re-heated microstructure D (x 150)	126
Fig(4.3.6) Photo-micrograph of re-heated microstructure E (x 150)	126
Fig(4.3.7) Photo-micrograph of re-heated microstructure F (x 150)	127
Fig(4.3.8) Photo-micrograph of re-heated microstructure G	127

(x 150)

Fig(4.5.1.1) Typical form of load versus clip gauge opening curve	128
Fig(4.5.1.2) Offset method to determine amount of plastic deformation	128
Fig(4.5.2.3.1) Mn% and Ni% in order of P_{gy} (all compositions)	129
Fig(4.5.2.3.2) Mn% and Ni% in order of P_{gy} (1%Mn)	129
Fig(4.5.2.3.3) Mn% and Ni% in order of P_{gy} (0.6%Mn)	130
Fig(4.5.2.3.4) Mn% and Ni% in order of P_{gy} (1.6%Mn)	130
Fig(4.5.2.3.5) Mn% and Ni% in order of P_{gy} (0.0%Ni)	131
Fig(4.5.2.3.6) Mn% and Ni% in order of P_{gy} (1.5%Ni)	131
Fig(4.5.2.3.7) Mn% and Ni% in order of P_{gy} (2.5%Ni)	132
Fig(4.5.2.5.1) Comparison of Mn% and Ni% in order of σ_{max}	132a
Fig(4.6.1.1) Scanning electron micrograph of -105°C fracture surface sample as-welded 7016 (x 2000)	132
Fig(4.6.1.2) Scanning electron micrograph of -105°C fracture surface sample as-welded 7016 (x 2000)	133
Fig(4.6.1.3) Scanning electron micrograph of -105°C fracture surface sample as-welded 7016 (x 2000)	133
Fig(4.6.1.4) Scanning electron micrograph of -105°C fracture surface sample as-welded 7016 (x 2000)	134
Fig(4.6.1.5) Scanning electron micrograph of -150°C fracture surface sample as-welded 7016 (x 2000)	134
Fig(4.6.1.6) Scanning electron micrograph of -150°C fracture surface sample as-welded 7016 (x 2000)	135
Fig(4.6.1.7) Scanning electron micrograph of -150°C	135

fracture surface sample as-welded 7016C1 (x 2000)	
Fig(4.6.2.1) Scanning electron micrograph of -150°C	136
fracture surface sample re-heated 7016 (x 2000)	
Fig(4.6.2.2) Scanning electron micrograph of -150°C	136
fracture surface sample re-heated 7016C1 (x 2000)	
Fig(4.6.3.1) Scanning electron micrograph of -150°C	137
fracture surface sample re-heated A (x 2000)	
Fig(4.6.3.2) Scanning electron micrograph of -150°C	137
fracture surface sample re-heated C (x 2000)	
Fig(4.6.3.3) Scanning electron micrograph of -150°C	138
fracture surface sample re-heated D (x 2000)	
Fig(4.6.3.4) Scanning electron micrograph of -150°C	138
fracture surface sample re-heated E (x 2000)	
Fig(4.6.3.5) Scanning electron micrograph of -150°C	139
fracture surface sample re-heated F (x 2000)	
Fig(4.6.3.6) Scanning electron micrograph of -150°C	139
fracture surface sample re-heated G (x 2000)	

The effect of manganese and nickel on the cleavage fracture strength of ferritic weld metal

By Andrew Robert Brian Sandford

ABSTRACT

All weld metal test pieces were produced from two commercial and six experimental 7016 type electrodes, each having different contents of manganese and nickel. These were tested in three point bending over a range of depressed temperatures in a cryostatic cell of the author's devising. Notched samples were used to obtain values for the cleavage fracture strength. This was calculated by reference to slip line field theory from the fracture load at the test temperature where fracture was coincident with general yielding. The commercial electrodes were first tested in the as welded condition and all eight electrodes were then tested after a heat treatment designed to give a microstructure similar to that found in re-heated weld metal. Notched and pre-cracked samples were then tested in the heat treated condition to determine K_{IC} values. Fracture surfaces were examined by scanning electron microscope and grain size measurements made by optical microscopy. Lower shelf impact energy measurements were also made.

The results showed that both manganese and nickel individually increased the cleavage fracture strength. In combination the best cleavage properties were given by alloying contents of 1.0% manganese and 1.5% nickel increasing alloying beyond this level had a detrimental effect. The mechanism for this was a combination of grain size effects, changes in the slip characteristics of the material, the size, distribution and nature of inclusions and the effects of alloying on grain boundary and matrix/inclusion cohesion. In re-heated material at the test temperatures studied the plane strain fracture toughness is influenced by similar factors to those which determine cleavage fracture strength.

1. INTRODUCTION

Welded steel structures play a vital role in modern engineering. Whether the finished product is a ship, a pressure vessel, an office block or an offshore oil platform a thorough knowledge of the mechanical properties of the weld and its associated heat affected zone is vital to safe design and the continuing integrity of the structure.

The development of the North sea oil industry in particular created a demand for welding consumables which could produce joints with a high toughness at low temperatures at the same time as satisfying the need for weldability, corrosion resistance and strength.

In the formulation of alloys to meet these requirements the manufacturers of welding consumables began to pay increasing attention to the relationship between these properties, the weld metal composition and the microstructure of the weld which was produced. Although many of the results agreed with those established for wrought materials there were interesting and significant differences.

By its very nature weld metal is a heterogenous non-equilibrium material. A variety of microstructure not normally seen in wrought metal may be produced as a result of the weld thermal cycle. Segregation, inclusions, dissolved gases, porosity and residual stresses will all result in a material which cannot adequately be described in terms of wrought alloys.



It became clear to electrode designers that one of the most important factors in determining the toughness of as deposited weld metal was the proportion of the non-equilibrium phase acicular ferrite.

If the manganese content was increased then up to a certain point this was beneficial to the properties of the material as the amount of acicular ferrite produced increased. However, if too much manganese was added the improvements in the mechanical properties were counter-acted by increased hardenability and the associated possibility of hydrogen induced cracking. Nickel was known to have a beneficial effect on the toughness of iron in wrought materials and so this led to an interest in electrodes with both manganese and nickel additions.

It should also be pointed out that the promotion of toughness by increasing the amount of acicular ferrite is only appropriate to as-deposited weld metal. In multi-run welds the as-deposited material will be re-heated, possibly a number of times, and the acicular ferrite structure will be transformed to a structure consisting of ferrite and pearlite. It is therefore clear that the other effects of alloying on the properties of the material are of the greatest importance.

Various suggestions have been made as to the mechanisms whereby manganese and nickel can promote toughness and these are



considered in depth in section 2.0. In brief these effects mostly relate to solid solution strengthening, the effects of these alloying additions in combination with carbon, grain size and microstructural effects and their influence on dislocation behaviour.

What becomes clear from this study is that some of the effects of these two alloying additions are complementary and some counteractive. There appears to be an optimum level of alloying for these elements when they are combined in a ferritic weld metal which gives the greatest benefit with the least detrimental characteristics.

The starting point for this research is therefore the consideration of how these alloying additions work together to improve the toughness of the weld metal produced.

The toughness of a material, in other words its capacity to absorb energy during fracture, is commonly regarded as one of the most important criteria in determining its suitability for a particular application. Traditionally this was studied by measuring the energy absorbed in impact tests on notched test-pieces. These tests were carried out over a range of temperatures producing a graph of energy absorbed against test temperature. For ferritic materials the plot characteristically shows a transition from high temperature, high energy ductile behaviour to low temperature, low energy brittle behaviour. This transition is often characterised by a single point, the ductile brittle

transition temperature (DBTT) which can be specified in a number of ways. These results have only an empirical value however, and despite many attempts can not convincingly be related to any fundamental material parameters.

A major part of electrode design in the past has been the modification of the shapes of these curves by alloying. This may be either to lower the transition temperature, to modify the upper and lower shelf energies or to flatten the curve producing a potentially less disastrous transition. It can not be denied that this approach has led to the development of excellent welding alloys but it reveals nothing about the fundamental processes which determine the changes in properties.

In this research the intention was to examine the fracture behaviour of manganese and nickel bearing ferritic weld metal in terms of a fundamental parameter. In low temperature fracture perhaps the most fundamental parameter is the cleavage fracture strength.

Cleavage can be characterised as fracture by the separation of atomic layers along certain clearly specified and typical crystallographic planes and in ferritic steels occurs when a critical value of principal tensile stress is exceeded. This value is known as the cleavage fracture stress (σ_F). In ferritic steels the initiation of cleavage is a dislocation dependent phenomenon and is slip induced. Cleavage fracture of ferritic steels is

discussed at length in section 2.4.

Since the cleavage fracture strength is a material parameter its relationship to fundamental measures of toughness can also be assessed. A range of such parameters has been developed through the study of fracture mechanics. The most widely used of these concepts is that of plane strain fracture toughness. This is discussed in section 2.3.2 and provides a description of a critical stress state at which fracture will occur at the tip of a theoretically atomically sharp crack. At low temperatures where cleavage is the dominant failure mode it might be expected that a relationship could be observed between the cleavage fracture strength and the plane strain fracture toughness.

The objectives of this research can therefore be defined as follows:

- *To investigate the effects of varying amounts of manganese and nickel on a fundamental material parameter of ferritic weld metal, namely the cleavage fracture strength.*
- *To investigate the mechanisms of these effects*
- *To relate these observations to other material parameters.*

2. LITERATURE SURVEY

2.1 Introduction

The nature of the welding process, involving as it does high rates of heat flow, mass transfer at elevated temperatures and the possible entrainment and dissolution of gases, leads to an as-welded material which is inherently complex.

Since the welded joint can be considered to be of key significance in the integrity of modern fabrications, an understanding of the factors affecting the mechanical properties of these welds is of immense importance for safe design.

One of the first steps towards this understanding was the development by Rosenthal in 1935 (1) of equations which described the flow of heat from a moving point source. These were found to be generally valid in describing the distribution of temperature around a welded joint and thus predictions could be made as to how the weld thermal cycle would affect the parent material. Since that time many attempts have been made to use this type of approach to predict the size and shape of the weld deposit, an area which has been thoroughly reviewed by Shinoda and Doherty (2).

The use of finite element methods of analysis has been developed to refine these original equations to take account of such things as phase transformations eg (3) and comparisons have been made between solutions derived from Rosenthal equations, numerical approaches and practical observations. Thus the thermal cycle



experienced by the weld and surrounding Heat Affected Zone (HAZ) can be described.

However, as the weld metal cools rapidly from the molten state non-equilibrium structures are certain to be produced on solidification and during subsequent cooling.

At the fusion line with the parent material some dilution will occur and there will be grain growth in the parent metal. The first weld metal to solidify will do so epitaxially from these grains. These first grains to solidify will be of a similar size and composition to those of the parent metal (4).

In the remaining molten weld pool with an $\langle 100 \rangle$ direction parallel to the steepest temperature gradient, it will outgrow those with a less favourable orientation. Thus as the fusion boundary moves forward grains will continue to grow in a columnar fashion.

Each grain will itself have a sub-structure due to micro-segregation. This micro-segregation depends on the solute front in the weld metal which in turn is influenced by the solute content and a parameter G/R where G is the temperature gradient in the direction of solidification and R is the rate of advance of the solute front. Thus the primary solidification structure is already quite complicated in nature. In the case of ferritic steels this situation is further complicated by phase transformations on cooling.

Widgery and Saunders (5) carried out an examination of the



solidification process in steel weld metals, studying the relationship between solidification structures and that of the finally transformed material. This research was later expanded by Abson and Dolby (7) in the light of new research. The principal findings of this research are examined in detail in section 2.2. Widgery categorised the phases formed in the final weld metal into four types (8) (9). These were pro-eutectoid ferrite, lamellar component, acicular ferrite and a general category of other constituents such as carbides, martensite, inclusions etc.

This scheme of categorisation was later revised by Abson and Dolby (10) to give the following descriptions of micro-structural constituent - grain boundary ferrite (GF), polygonal ferrite (PF), acicular ferrite (AF), ferrite with aligned M-A-C (ferrite containing martensite-austenite or carbide phases) (AC), ferrite carbide aggregates (including pearlite) (FC) and martensite (M). Thus the cooling and transformation sequence for a ferritic steel weld metal can broadly be described as follows:

The first metal to solidify is BCC (delta) ferrite which with a small decrease in temperature transforms to FCC austenite (gamma). This may retain an as-cast appearance, even though the original (delta) ferrite grain boundaries are not preserved. This transformation will be complete by the time that the weld has dropped in temperature to about 1300°C.

The next transformation will take place between 950°C and 720°C when (alpha) ferrite starts to form at the (gamma) grain



boundaries. This grain boundary ferrite (GF) will grow to form a continuous network around the (gamma) grains. With further cooling pearlite, an aggregate of (alpha) ferrite and cementite, categorised by Abson and Dolby (10) as FC, will begin to form.

Due to the cooling rates associated with weld metal, the cementite (Fe_3C) will not necessarily be in a lamellar form, but may exist as rods or spheres.

Two further types of ferrite then begin to form, namely ferrite side-plates which grow from the grain boundary ferrite and equiaxed grains of polygonal ferrite (PF).

The next phase to form, acicular ferrite (AF), is widely considered to be of great benefit to toughness, and forms inside the remaining austenite grains. Since the transformation temperature is low a very fine structure results.

As the temperature continues to drop the final austenite to transform produces a martensite/austenite/carbide complex (M-A-C). This phase is believed to have a deleterious effect on toughness with the thin, angular plates acting as stress raisers.

The weld metal micro-structure is further complicated by the presence of dissolved gases in the molten weld metal and the products of reactions between the weld metal and slag producing agents.

For Manual Metal Arc (MMA) welding the slag/metal reaction occurs at the interface between the molten tip of the core wire and the



coating. This reaction may be used by the electrode manufacturers to add alloying materials to the weld metal as well as for deoxidation. This is important since oxygen and other gases may be absorbed into the weld pool at this stage. Deoxidants and metal are transferred to the weld pool, and the inclusions resulting from reactions involving these in the weld pool can later be important in the nucleation of both phase transformations and fracture.

The absorption of gases into the weld pool can lead to problems of porosity and cracking after solidification. Despite the use of shielding agents in the electrode coating nitrogen and oxygen can be drawn from the air into the weld metal and hydrogen can be present as a result of the dissociation of moisture in the air or even in the electrode coating.

Nitrogen will have dissociated from the molecular to the atomic form in the arc and thus reacts more intensively with the weld metal (11). In the solidified weld it can be present either as nitrogen in porosity, in the combined form as an iron/nitrogen interstitial solid solution, possibly super-saturated, or in the form of nitrides. Each of these can affect the strength and toughness of the weld. Porosity itself does not necessarily affect the integrity of the weld but will reduce the effective cross section. Dissolved nitrogen can increase the upper yield strength, whereas FeN has been found to reduce impact toughness and increase hardness.

There is however some evidence (12) to suggest that in



conjunction with manganese, toughness may be increased as a result of improved grain boundary ductility.

Hydrogen can form porosity in the weld and may diffuse into the HAZ where it can induce cracking. Low hydrogen basic electrodes have now been developed which can, with correct use, eliminate most problems of hydrogen-induced cold cracking.

Weld metal oxygen is controlled by de-oxidants in the electrode coating. These de-oxidising reactions result in non-metallic inclusions which are dispersed in the weld metal. The inclusion type and size distribution has been shown (13) to have an important effect on the transformation characteristics of the weld metal, in particular on the acicular ferrite field of the continuous cooling transformation curves.

This effect is, however, not solely due to the oxygen regime, but depends also on the other elements present. Among the alloying additions which may be added to ferritic weld metal, nickel and manganese are widely recognised as being beneficial to toughness. Various suggestions have been made as to the roles they can play in this context. One major factor appears to be the ability of these elements to refine the grain structure of both as-cast and re-heated weld metal. In his work on manganese (14-18) Evans found that its presence had a three-fold effect, in that it:

- a. caused the proportion and refinement of acicular ferrite to increase at the expense of the less desirable pro-eutectoid



ferrite

- b. refined the coarse grained region of re-heated weld metal
- c. refined the grain size of the equi-axed fine grained zone of the re-heated weld metal.

Evans found that optimum values for impact and CTOD (Crack Tip Opening Displacement) were obtained at a manganese content of 1.5% but at higher levels, the increased yield strength acted to reduce toughness. A more complete treatment of the role of manganese will be given in section 2.2.

Taylor and Evans (19) showed that with the addition of nickel, the optimum manganese level was progressively decreased but that for practical reasons a combination of 1% nickel and 1.2% manganese gave the best combination of toughness and deposition rate.

Possible reasons for the beneficial effects of nickel on toughness were suggested to be a reduced prior austenite grain size and consequently refined acicular ferrite and the elimination of grain boundary ferrite. Many questions however, remained unanswered about the combined effects of manganese and nickel.

Since the introduction of welded steel fabrications for structural applications, attempts have been made to define and predict resistance to fracture. An important concept here is that of toughness, which can be defined as a material's ability to resist the rapid propagation of a crack. In a brittle material little energy is absorbed during fracture and rapid crack growth is not impeded. In a tough material energy is



absorbed in the form of plastic deformation which impedes the progress of the crack.

The traditional method of comparing the toughness of different materials has been to use an impact test on standard notched samples. In this technique, the most commonly used of which is the Charpy V notch method, a weighted pendulum is used which is raised to a standard height and allowed to fall, striking and breaking the sample.

The height to which the pendulum rises after impact gives an indication of the kinetic energy which has been absorbed in fracture. Tests are carried out over a range of temperatures and the fracture energies for each temperature plotted.

Since with ferritic steels there is a temperature at which the fracture mode changes from ductile to brittle, these curves can give a useful indication of the conditions in which the material will be safe to use. These results are however, empirical and cannot readily be related to fundamental material properties. A large part of welding electrode design has been aimed at the modification of these curves by alloying additions. The shape of these curves has been changed to reduce the ductile-brittle transition temperature (DBTT), to modify the upper and lower shelf energies and to flatten the curves to give a less potentially disastrous transition.

To try and develop a more fundamental method of assessing toughness, a variety of fracture-based approaches have been adopted.



The plane strain critical stress intensity factor K_{IC} is a material constant and describes the critical value for local stress distribution at the tip of an infinitely sharp crack above which that crack will propagate.

The method uses a notched and fatigue pre-cracked specimen which is tested in slow bending or tension. The specimen geometry and test conditions are closely specified to ensure that plane strain conditions prevail, and that the value obtained is valid. This is to ensure that no plastic strain occurs since the theory strictly applies to a linear elastic solid only.

As the ductility of the material under test increases, the test piece needs to become larger to ensure plane strain conditions and this can be a practical limitation to the method. Another drawback is that it can only be determined with certainty after the test is complete whether the test has been valid.

To overcome the situation where plastic deformation is inevitable the CTOD method of assessing toughness has been developed. This method again uses a notched and fatigue pre-cracked specimen which is tested by slow bending. The difference between this and the K_{IC} test, in practical terms, is in the interpretation of the results.

In the current investigation research is concerned with the brittle mode of fracture, which normally occurs at low temperatures. The fracture mechanism under study is that of



cleavage. Cleavage can be characterised as fracture by the separation of atomic layers along certain clearly defined and typical crystallographic directions. In ferritic steels cleavage occurs when a critical value of principal tensile stress is exceeded. This value is known as the cleavage fracture stress (σ_F).

Cleavage fracture generally proceeds in two stages, cleavage crack initiation, and then, once a critical flaw size has been reached for the applied stress, crack propagation. In practice cleavage can be associated with limited plastic deformation and should therefore be differentiated from what is regarded as brittle fracture in engineering terms.

In ferritic steels cleavage is a slip-induced dislocation dependent phenomenon. All models for cleavage initiation in these materials propose dislocation pile-ups as a necessary first stage in the process. This may either be at intersecting slip planes (20) where the pile-up forms a wedge shaped crack, or at grain boundaries where the applied stress produced may cause brittle grain boundary material to crack. This cracking may occur at an interfacial separation due, for example, to segregated phosphorus (21) or may occur in brittle particles such as carbides precipitated at the grain boundary (22).

The dependence of cleavage strength on carbide size has been demonstrated (21) and so it is currently believed that the grain boundary model of cleavage initiation is more appropriate (22)



(23) and that the likely mechanism is the cracking of grain boundary carbides.

Cleavage initiation is less likely if the applied stress from the dislocation pile-up can be accommodated by plastic flow of material around the brittle carbides. Cracked carbides have been shown to act as cleavage initiators and these cracks propagate at a critical stress level under the combined effects of the dislocation pile-up and the resolved applied stress. Thus, cleavage is less likely when lower yield stresses prevail.

This is the case when the free movement of dislocations is possible due to a low strain rate and high temperatures. The effect of alloying on the slip characteristics of the material can therefore be seen to be of great importance in the cleavage process.

2.2 Welding Metallurgy and the Influence of Alloying Additions

As was shown in Section 2.1 the factors influencing the toughness of weld deposits are far less easily examined in a quantitative manner than normal wrought materials. However, the factors affecting toughness can still be categorised as:

- solid solution effects
- grain size effects
- precipitation effects
- dislocation sub-structure effects.

In a survey carried out by the Welding Institute for BOC Murex (24) and quoted by Judson and McKeown, the effects of a wide range of alloying additions were summarised as follows:

The effect of solid solution strengthening on yield and tensile strength decreases approximately in the order: carbon, nitrogen, phosphorous, titanium, vanadium, silicon, manganese, copper, aluminium, molybdenum, nickel, chromium.

Nitrogen, phosphorous and sulphur all have a detrimental effect on toughness and should therefore be kept to the lowest possible level.

High levels of both silicon and oxygen can be prejudicial to toughness although there may be an optimum level of the two elements which is above zero.

In the case of some elements toughness increases with increasing additions at low levels with the strength also increasing but

then a maximum is reached after which it begins to decrease.

In the weld metal microstructure there is no continuous matrix of material as with wrought materials and so the grain size effects depend also on the phases present. It is generally recognised that in CMn type weld metals in the as-deposited state a high proportion of fine-grained acicular ferrite promotes toughness but this also depends on the proportion and distribution of such brittle phases as martensite and carbides. The presence of brittle inclusions which may initiate cleavage and the slip characteristics of the material which determine the extent of dislocation pile-ups at brittle phases and inclusions are also an important factor in the overall picture.

Even with a constant composition of filler rod and parent material results can be influenced to a great extent by procedural variables. Particularly important here are heat input, degree of re-heating in multi-run weld metal and pre- or post-weld heat treatment. This is to leave aside any problems associated with bad welding practice.

2.2.1 The Influence of Alloying Additions on Weld Metal Microstructure

The microstructure which develops in a steel weld metal has been discussed in Section 2.1 in terms of the sequence of formation of the various phases. The temperatures of formation for the various phases were determined by Choi and Hill (25) to be as follows:

1000 - 600°C Primary ferrite at austenite grain boundaries
750 - 650°C Ferrite side plates also at the austenite grain boundaries
below 650°C Acicular ferrite within the prior austenite grains
below 500°C A bainite-like lath structure forms.

It has been shown by various researchers that the oxygen regime prevailing in the weld deposit has a decisive effect on the proportions of these various phases and hence toughness (7,13).

Three broad types of microstructure have been linked to three bands of oxygen content:

In high oxygen weld metal (>0.06%) the resultant high inclusion content restricts the size of the austenite grains in the as-deposited weld metal (26-29). The structure of the resulting ferrite is mostly Widmanstätten side plates with micro-phases strung out between the ferrite laths. It is considered that the nucleation sites for these ferrite laths are oxide inclusions at the austenite grain boundaries (13).

Acicular ferrite is not produced due to the high start temperature and rapid rate of transformation. However, if the ferrite grains fail to grow to mutual impingement, bainite may form between the laths. With oxygen contents of around 0.03% inclusions are formed which act as nucleants within the grains leading to acicular ferrite as the major micro-structural

constituent. Grain boundary ferrite and ferrite side plates are still present and form before the acicular ferrite.

The acicular ferrite laths normally grow to mutual impingement (13) after which the pools of austenite trapped between them may transform to martensite, upper bainite or ferrite-carbide aggregate (30,31). The formation of a significant amount of bainite may occur where there are insufficient ferrite nucleants to allow mutual impingement of ferrite laths to occur. The transformation start temperature for each phase may be affected by alloying additions. It has been shown that the start temperature for the formation of grain boundary ferrite decreases with increasing alloy content.

If a low oxygen condition prevails, the formation of laths of intragranular acicular ferrite will be inhibited and the microstructure will consist predominately of lamellar colonies of ferrite with elongated microphases. This constituent may be known as either bainite or lath ferrite.

The theoretical calculations of Ricks et al (32,33) have suggested that once grain boundary nucleation sites for ferrite have been exhausted then inclusions were the next most preferred sites, with large inclusions being more favoured than small ones. The role of these intragranular inclusions as nucleation sites has been observed by several workers and has been reviewed by both Pargeter (34) and Devillers et al (35).



In an extensive series of publications on carbon-manganese weld metal (14-18), Evans has shown that additions of manganese increased the proportion of acicular ferrite at the expense of grain boundary ferrite in as-deposited regions and also decreased the grain size in the fine-grained re-heated regions. Manganese exhibits a marked carbide-forming tendency and acts to reduce the growth rate of ferrite due to co-segregation with carbon (36). In reheated material pearlite forms preferentially at areas high in manganese which at the same time refines its structure.

One of the major micro-structural effects of nickel is to act as a refining agent on the structure of re-heated ferrite and pearlite due to its action as an austenite stabiliser. According to Taylor and Evans additions of nickel refine the acicular ferrite structure by depressing the transformation temperature, as is also the case in grain refined regions (37).

The proportion of acicular ferrite is, however, not necessarily increased (Taylor and Evans *ibid*) and in association with 1% of manganese a nickel content of 3.5% can promote the formation of ferrite with aligned second phases.

Section 2.2.2 The Effect of Alloying on Weld Metal Toughness

As was stated in the introduction to this section, toughness depends on several, possibly competing, effects. The effects of microstructure on toughness can, in the most part, be ascribed to

grain size related changes or the presence of brittle phases which may act as fracture initiators. Again, most of the phenomena described apply to the as-deposited microstructure.

In this work the majority of the research was concerned with reheated material although here too, grain size refinements and cleavage initiation are the most important micro-structural concerns. For reheated material, since the microstructure is more amenable to interpretation, the other factors affecting toughness can more easily be examined. This section will therefore discuss both as-deposited and reheated structures.

With reheated structures there is a progressive decrease in the prior austenite grain size with decreasing reheat temperature which in turn increases the proportion of grain boundary ferrite to the intra-granularly nucleated acicular ferrite. If the material is heated above the A_3 temperature the prior austenite grain size is very small and thus the ferrite formed almost all equi-axed with carbide/ferrite aggregates present as pearlite so that as-deposited terminology is no longer appropriate.

Section 2.2.3 Strengthening Mechanisms

It could be stated as a generalisation that increased tensile strength is associated with a decrease in toughness characteristics since the ability of the material to undergo plastic

deformation and hence absorb energy is thus reduced. It can, however, be possible to increase strength and toughness together if other factors become significant.

manganese has been shown by Pickering (38) to have a moderate solid solution strengthening effect in wrought steels which is of the order of $30\text{MNm}^{-2} / \% \text{ manganese}$. In weld metals a greater effect has been observed with values of $50 - 100\text{MNm}^{-2} / \%$ being reported (7,14,15,39). Evans has shown (17) that this also depended on the interpass temperature with a more marked effect at lower temperatures. Thus, manganese can be seen to have a greater effect on strength than simply that due to solid solution hardening.

It is likely that a significant factor here is the grain refining effect observable in both as-deposited and reheated regions. Work on single run welds (9,42) suggests that the increased proportion of acicular ferrite is of particular importance.

For nickel Pickering also reports a solid solution strengthening effect, but again work on weld metal (39,42) shows a greater rate of increase in strength with nickel content than can be explained in these terms alone. Thus it seems again that solid solution strengthening is of much less importance than grain size effects although the possibility of a small degree of precipitation hardening also exists .

Several workers have examined the effect of grain size on the yield and tensile strength of both single- and multi-run welds for a constant deposit composition (17,40,43). The results have generally been seen to fit the Hall-Petch relationship:

$$\sigma = \sigma_0 + kd^{-1/2}$$

Where σ is the yield stress and σ_0 and k are constants.

In these experiments grain size was varied by changing the interpass temperature or post-weld heat treatment. The constant σ_0 , known as the friction stress, was found to have a negative value, this being explained by the increasing importance of dislocation related effects with decreased grain size. If further heat treatment is carried out to remove the dislocation sub-structure these effects are eliminated.

It has been shown by Dolby (44,45) that if alloying increases the tensile strength but does not refine the microstructure in any way, then the toughness of the material is reduced. As a counterpoint to this, Garstone and Johnson (46) showed that for two MMA deposits with the same composition but differing grain sizes (achieved by different normalising temperatures) the smaller grain size gave increased toughness.

Section 2.2.4 Toughness of Ferritic Weld Metal

The factors affecting weld metal toughness in ferritic steels are the yield stress, the ferrite grain size, the presence and nature of any nucleators for cleavage and the matrix resistance of the ferrite to cleavage. The latter two are those with which this research is primarily concerned since re-heated material was the main area of study.

The effects of alloying with manganese and nickel on the room temperature tensile strength have been studied by King, Jarman and Judson who concluded that nickel in particular reduces yield strength and ductility parameters at the same time as increasing the tensile strength. Manganese also increases strength and tends to obscure some of these effects. For reasons of practical application the majority of research on the relationship between alloying and toughness has concentrated on as-deposited weld metal where microstructural effects, and in particular the importance of acicular ferrite, have been stressed.

Acicular ferrite has been demonstrated to have good resistance to cleavage because of its fine structure, whereas large regions of grain boundary ferrite with a coarse structure reduce toughness. Ferrite with aligned secondary phases also has a detrimental effect on toughness since cleavage can initiate at brittle regions within these phases. At levels of around 1% manganese, it has been shown by several authors to have a beneficial effect on impact toughness with increasing amounts.

The effect on the Charpy transition temperature has been studied by Widgery (48) and Sakaki (39) who found the 50% fracture area transition temperature to be reduced by 40K / % Mn and 30K / % Mn respectively. Evans (14,15,49) showed that for all weld metal deposits (MMA) of 7018 electrodes at 1kJ/mm an optimum manganese content of about 1.4% Mn was observable for both Charpy and CTOD tests. In later work where the silicon content was also varied, Evans found the optimum value to be about 1.8% (50,51). This has been explained by Dolby (44,45) as being due to a continued increase in strength after all possible microstructural improvement has been achieved leading to a decrease in toughness with continued additions. A further factor in the decline of toughness may also be due to the formation of martensite.

In vertical up welds both Abson and Taylor found the optimum manganese value to be 1.7% for Charpy toughness and an optimum of 1.8% for CTOD was found by Dolby. As discussed in section 2.2.1 the presence of manganese at these levels refines the acicular ferrite structure and increases the proportion of that phase. Evans found (14,15) a substantial reduction in the amount of grain boundary ferrite and little effect on the proportion of ferrite with aligned MAC.

Taylor (53), Barritte et al (29) and Abson (52) found similar effects on the acicular ferrite and grain boundary ferrite but found that the proportion of ferrite with aligned second phase was also reduced. Morigaki (54) found similar results in the as-

deposited regions of multirun welds. The refining effect of manganese on re-heated weld metal was found by Evans (14,15) and Widgery (9).

Manganese can also act in other ways to improve toughness. From studies of wrought steels it has been shown that in body centred cubic (BCC) iron, carbon is surface active and its presence in the interstitial solid solution improves the cohesion of the grain boundary. In the absence of manganese any excess of carbon above the solid solubility limit would be present at the grain boundaries forming an intergranular network of brittle cementite (Fe_3C). Manganese is absorbed at the interfaces of cementite, austenite and ferrite increasing the cementite-ferrite interfacial energy and preventing the spread of cementite along the grain boundary (55). The presence of grain boundary carbides is particularly detrimental to toughness since they can provide sites for cleavage initiation (56).

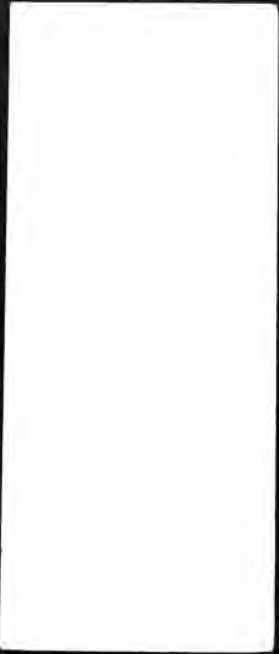
The presence of manganese can also modify the deformation characteristics of ferrite by reducing the number of ferrite sub-boundaries (57). It can also affect cross-slip of dislocations and the length of dislocation pile-ups at grain boundaries (55,58).

These observations on wrought materials may be of some significance in the completely re-heated structures studied in this research.

Nickel is generally recognised as having a beneficial effect on toughness. Both Sakaki (39) and Ohwa (59) demonstrated an increase in toughness with increased nickel in levels up to 1.5%. They measured the temperature for an absorbed impact energy of 20J and found a decrease with nickel of 16K / % nickel. Bosward and John (41) also carried out work which demonstrated the beneficial effects of higher nickel contents at -50 and -70°C as a result of increased amounts of acicular ferrite.

Mentink (60) observed that nickel additions reduced the amount of scatter in impact tests and this can also be seen in the results of Morigaki et al (61). Nickel refines the structure of acicular ferrite (37) and the grain refined regions by lowering the transformation temperature due to its action as an austenite stabiliser (58,62,63). The proportion of acicular ferrite may not, however, be increased.

In addition to its effect on the microstructure of the deposit, nickel can also contribute to the toughness properties of the weld by improving the properties of the ferrite matrix. The presence of nickel increases the stacking fault energy and the ability of dislocations to cross slip. This may promote toughness, either by preventing dislocation dissociation or by spreading the shear misfit of (100) edge dislocations. Their effectiveness as crack nuclei is thereby reduced and the initiation of cleavage cracks in the ferrite becomes more difficult (63).



The presence of nickel in solution produces centres of strain which can trap interstitials such as carbon and nitrogen which prevents them assisting in dislocation locking (58). Nickel is not a carbide former and acts on carbon to reduce its diffusivity whilst enhancing its activity. This is only of benefit in the absence of carbide formers such as manganese since they reduce the amount of carbon in solution and the action of nickel may then contribute to a decrease in grain boundary cohesion (58). The decreased carbon solubility can also act to produce coarser precipitates, which although reducing strength may reduce the number of centres of micro-void coalescence during ductile failure.

In combination some of the effects of manganese and nickel might appear to be counteractive whereas others are complementary.

Taylor and Evans (37) and Judson and McKeown (64) both observed the interactive effects of manganese and nickel in MMA deposits and showed that at higher manganese levels (1.4, 1.6 and 1.8%) increasing nickel above about 1.0% led to a reduction in toughness. With about 1.6% manganese an increase in nickel from 0 to 3.5% leads to a slight deterioration in upper shelf toughness but improves low temperature properties. On vertical up welds Morigaki et al found that with an arc energy of 5kJ/mm an optimum nickel content is observed which decreases as manganese is raised from 0.9 to 1.6% (61). Mentink (60) found an optimum balance of manganese and nickel to be 1.6 and 1.8% respectively. Pechennikov et al (65) found that for MMA deposits containing 1.2% manganese and 1.3% nickel an impact toughness equivalent to a Charpy value of 55J was obtained at -80°C.

As was previously stated, nickel refines acicular ferrite without necessarily increasing the amount of that phase. At a manganese level of about 1% the presence of 3.5% nickel in MMA deposits was found to lead to the formation of ferrite with an aligned second phase leading to a reduction in toughness. An interaction between nickel and manganese leading to improved toughness has been observed in submerged arc welds by Hirabayashi et al (66) where impact values equivalent to 109J at -62°C were observed for manganese and nickel contents of 1.35 - 1.7% and 0.9 - 1.6% respectively. It may well be that this is also applicable to MMA deposits.



A critical combination of manganese and nickel is also required to prevent interstitials such as carbon and nitrogen from assisting in dislocation locking (55). This improves toughness by decreasing the density of un-arrayed and unlocked dislocations. The mechanisms for the interaction of manganese and nickel are however still not clear. It is hoped that this study, concentrating as it does on reheated material will allow further light to be shed on this area.

Section 2.3 Approaches to Toughness Characterisation

Section 2.3.1 The Charpy V Notch Method

As was first mentioned in Section 2.1 the method traditionally chosen to examine and compare toughness has been the notched impact test, commonly the Charpy V notch method, which can produce ductile/brittle transition curves roughly comparable to those found for the bulk material in service. This transition point may be characterised as the temperature at which a given energy (eg 27J) is absorbed by the testpiece, or alternatively defined in terms of the point for 50% crystalline fracture as determined by visual inspection. The method has the advantages of being relatively rapid, easy to carry out and cheap and no doubt has a role in ranking materials in toughness order and for quality assurance purposes. It remains, however, an empirical method which cannot be related convincingly to any fundamental material parameters.

The notch produced can only act as a stress concentrator for the

purposes of the test and does not relate to real cracks which may occur in fabricated structures. Because of the bluntness of the notch the stress field is such that a relatively large volume of the material is sampled. This leads in turn to a considerable degree of scatter in the results.

The strain rates obtained in impact are of the order of $10^5 - 10^6$ times those observed in a standard tensile test which can dramatically affect the local yield stress of the material and again produce scatter in results. Another drawback to the method is the small size of the testpiece which may be misleading when compared to the size of the weldment under examination.

A considerable body of work has, however, been carried out in an attempt to make impact testing results more meaningful. Towers, for example (67) examined the effects of reducing thickness of Charpy specimens, finding that with thinner samples the ductile/brittle transition temperature was reduced.

Wilshaw and Pratt (68) studied the mechanics of deformation in the three point bending of Charpy specimens and varied the striker velocities from 0.05 to 30,000 cm/min within a temperature range of 100°C to -196°C and found that there was a transition from ductile tearing to internal cleavage at the notch root but that there was a bimodal energy regime in the region of slip-initiated cleavage and a decrease in fracture load associated with mechanical twinning. From these experiments they also identified a cleavage strength σ_{CS} which they defined as the maximum longitudinal tensile stress below the notch root to cause

cleavage. It was further proposed that this cleavage strength must be dependent upon some micro-structural deformation features which do not influence the bulk plastic properties of the material.

Similarly Neumann, Benois and Hilbert (69) examining the impact toughness of weld deposits produced from basic electrodes found a pronounced bimodal behaviour after the statistical analysis of over 4000 impact tests carried out between 20°C and -120°C. The bimodal behaviour was found to occur between -20° and -60°C and showed two quite distinct types of curve for absorbed energy versus temperature. The upper curve showed a mixed fracture mode with a distinct plastic component whereas the lower curve exhibited purely brittle failure. This bimodal behaviour was not affected by notch type or orientation, the cross-sectional weld structure or normalising heat treatments. Certain alloying elements at low concentrations caused this bimodal behaviour to continue at lower temperatures.

Rosenfield and Shetty (70) described the results of fracture toughness in the ductile brittle transition region of ASTM A508 steel and found similar problems as those found with Charpy testing, namely a combination of brittle and ductile behaviour resulting in experimental scatter. Both crack blunting and dimpled rupture are halted by unstable cleavage crack growth. At lower temperatures cleavage occurs during blunting whereas at higher temperatures cleavage occurs after stable crack growth. They suggested that this may be due to the presence of inclusions

and carbides which act as triggers for cleavage. It might be expected that under the 'instantaneous' conditions of impact testing these conditions would be aggravated.

In an attempt to obtain more information from the Charpy test various workers have attempted to instrument the tests to give dynamic measurements of the load as a function of time. Almond and Embury (71) for example, used this approach on low carbon steel testpieces over the temperature range of 150 to -196°C and found that the results obtained for load versus temperature were similar to those obtained from notched bend tests. An attempt was also made to correlate these results with variations in microstructure.

Sandstrom and Bergstrom (72) examined the relationship between the Charpy V notch transition temperature in mild steel and various material parameters. This took as its starting point the relationship defined by Knott (73) when T , the test temperature is equal to T_{cv} the ductile/brittle transition temperature, for the internal fracture stress σ_f namely:

$$\sigma_f = Q\sigma_y$$

where Q is a plastic stress intensification factor caused by the triaxial stress state below the notch root and σ_y is the yield stress at general yield. From this relation it was proposed that if Q could be determined and the temperature dependence of σ_f and σ_y are known an analytical expression for T_{cv} can be established. If the influence of grain size and other

parameters on fracture and yield strength are also known then it was proposed that the effects of these on T_{cv} could also be determined.

Other attempts had been made to achieve this (74,75), but Sandstrom and Bergstrom felt that the expressions obtained lacked well-defined physical significance and their ability to successfully predict the transition temperature was, in most cases, limited.

By a series of experiments including uni-axial testing and four point bending, backed up by SEM studies, the following relationship was determined for T_{cv} :

$$T_{cv} = \frac{T_0}{\ln(v/\dot{\epsilon}_0)} \ln \left[\frac{\sigma_0}{(\sigma_f / Q_{cv}) - \sigma_G} \right]$$

where Q_{cv} is approximately 1.94 if the Tresca yielding criteria is used, $\dot{\epsilon}_0$ is the strain rate below the notch root and estimated as 400 s^{-1} . σ_G is the non-temperature dependent component of the yield stress and T_0 , σ_0 and v are constants. These latter four are determined from uni-axial testing and σ_f from four point bending.

Thus it can be seen that if material parameters are known the ductile-brittle transition temperature can be calculated. It would seem unlikely that any useful results could be obtained by using the formula in reverse.

Section 2.3.2 Plane Strain Fracture Toughness

If a notched sample under uni-axial tensile stress is considered then this discontinuity produces a stress intensity profile with principal stresses σ_{xx} , σ_{yy} and σ_{zz} . If the material is ductile then plastic deformation will occur at the crack tip under the influence of the high stress intensity σ_{yy} and the crack faces will move apart. The greater the ductility of the material then the greater will be the size of this plastic zone. If the material surrounding the crack or notch is sufficiently hard to restrict the growth of this plastic zone then secondary stresses will build up both at right angles to the plane of the discontinuity and parallel to the crack or notch face and a tri-axial stress state will prevail.

If the sample is thick enough the presence of a notch will lead to a tri-axial stress state which will increase the local yield stress of the material ahead of the crack. Such a condition is likely where the thickness or the hardness of the material is increased. If the maximum tri-axial stress at the crack tip exceeds the fracture stress of the material then the crack will grow.

Once the crack size is increased the fracture stress is effectively lowered and crack growth can accelerate. The stress distribution over a distance ahead of the crack is given by the equation:



$$\sigma_{yy} = \frac{K}{(2\pi x)^{1/2}}$$

where K is the stress intensity factor. This is dependent on the applied stress and for a thin disc-shaped crack with a diameter of 2c can be stated as :

$$K = \sigma_{\text{applied}} (\pi c)^{1/2}$$

If failure occurs at some critical value of applied stress then the parameter K becomes K_C . For opening mode loading this is K_{IC} which can be taken as a constant for a given material and is used to characterise the fracture toughness of the material. K_{IC} is dependent on temperature and strain rate and thus the validity limits and testing procedure need to be closely defined by a suitable standard such as BS 5447:1977.

This strictly relates only to a linear elastic material and where some plasticity occurs the CTOD method should be adopted. This is based on the amount that a crack can open under stress (δ) without the crack length increasing and can be related to K_C by the equation:

$$\left[\frac{K_C}{\sigma_y} \right] = \frac{\delta_c}{\epsilon_y}$$

where σ_y is the yield stress of the material and ϵ_y is the yield

strain. Test procedures for CTOD are specified in BS 5762:1979. Both these test procedures require a fatigue pre-crack to be introduced into the sample and require larger testpieces than the Charpy method, combined with the closely defined testing procedures and the possibility that a given test will prove invalid this makes the fracture toughness approach both more expensive and time consuming than Charpy testing.

The difference in results obtained by K_{Ic} testing and Charpy impact methods were highlighted by Ritchie, Francis and Server (76) who evaluated the toughness of AISI4340 steel at low and high austenitising temperatures by both methods. With an austenitising heat treatment at 1200°C instead of the more usual 870°C a two-fold increase in K_{Ic} was observed whereas the Charpy impact energy decreased. This was found to be due to the different effects of the blunt notch and the pre-fatigued crack on the fracture characteristics of the structure produced by the increased heat treatment temperature. This behaviour was tentatively ascribed to the larger effective root radius with sharp cracks as a result of the increased prior austenite grain size. The structure produced at 870°C was found to be more favourable to good Charpy results because of its larger critical fracture stress for failure. The authors suggested that on the basis of these results the toughness evaluation of a material should take into account both approaches, ie values for both sharp and rounded notches should be obtained.

It should be noted that the fracture toughness can be related to

the strain energy release rate G (sometimes called the crack extension force) with the critical strain energy release rate for the crack opening mode $G_{IC} = (K_{IC})^2 / E$, where E is the Young's modulus of the material.

For elastic-plastic fracture regimes K is no longer applicable and in this case the J integral approach may be used. This was developed by Eshelby (77) from an original definition by Rice (78) (79) to characterise general forces on dislocations and point defects in elastic fields using a static component of the 'energy momentum tensor'. J is a measure of the work input to a system and is independent of the path chosen to define the stress field. Load/displacement curves are produced to derive the empirical relationship of J to the increment of displacement at several crack lengths. The results obtained can be related to G and K for plane stress and plane strain.

Section 2.4 Cleavage Fracture of Ferritic Weld Metal

As has already been described in Section 2.1 cleavage in ferritic steels is a slip-induced dislocation dependent phenomenon with dislocation pile-ups being a necessary first requirement for cleavage initiation. Cleavage can be evaluated in terms of a critical value of principal tensile stress at which fracture occurs known as the cleavage fracture stress (σ_f).

Brittle fracture in steels normally occurs at low temperatures and/or high strain rates where energy dissipation by plastic flow is suppressed. The segregation of certain solute elements to



grain boundaries causing a brittle network of material to form can also change the fracture mode. Fracture by cleavage in steels can generally be thought of as a three stage process with the following steps:

1. Crack initiation, probably at a hard particle blocking a slip band (thus local yielding is required for initiation)
2. Propagation of the crack from the hard particle into the surrounding material at some critical value of principal tensile stress
3. Growth of the microcrack through the surrounding material.

Thus the cohesive energy of the material γ can be seen to be of importance. In an elastic-plastic material the major component here is plastic work which is the energy dissipated by dislocation motion at the crack tip during the stretching and breaking of bonds.

Following Kameda & McMahon(80), whether or not brittle fracture results from the cracking of a hard particle depends on the value of this plastic work, which they considered a fundamental material parameter controlling a material's resistance to brittle fracture. Although it was said to vary with the speed of propagation of the micro-crack the value required was that where the micro-crack exits the hard particle and enters the ferrite matrix.

In an analysis of the temperature dependence of cleavage fracture strength and fracture toughness, Kotilainen highlighted attempts to link the two (81). Starting from the equation of Yaroshevich and Ryvinka (82):

$$\sigma_y = \sigma_\mu + [\sigma_{y0} - \sigma_\mu]e^{-mt}$$

where σ_y = yield strength

σ_{y0} = yield strength at 0K

σ_μ = temperature independent component of yield strength

m = constant

t = absolute temperature

Kotilainen assumed that the cleavage fracture stress σ_{fc} is equivalent to the term σ_{y0} the yield strength at absolute zero. The specimen breaks when the maximum tensile stress σ_{yy} ahead of the notch tip reaches this value. This value can be calculated using the method of Green and Hundy (83) to be equal to $K\sigma_{GY}$ where K is plastic stress concentration factor and σ_{GY} the general yield stress and from this it is possible to solve the critical temperature at which σ_{GY} and σ_{fc} are equal:

$$T_c = \frac{1}{m} \ln \frac{\sigma_{y0} - \sigma_\mu}{\frac{\sigma_{y0}}{K} - \sigma_\mu}$$

Kotilainen then demonstrated the validity of the assumption that σ_{y0} is equivalent to σ_{fc} experimentally.

It has been shown by Hauser et al (84) among others that plastic deformation is a necessary precursor to cleavage. Therefore if the production of the required amount of plastic deformation is the critical step in the fracture process the cleavage fracture is mechanism controlled.

Whether or not this is the case can be determined by using the Griffiths and Owen (85) method of stress analysis to discover the smallest volume of the plastic zone and comparing it to microstructural parameters relevant to yielding and fracture. If the plastic zone for fracture is larger than say lath width and package size then fracture is not mechanism controlled and the maximum stresses below the notch at fracture represent the cleavage fracture stress.

Where steels have large discrete carbide particles cleavage is generally initiated at cracked carbide particles as shown by McMahon and Cohen (86) and Hodgson and Tetelman (87), and is broadly proportional to the reciprocal square root of the carbide thickness (Curry and Knott 88). Curry and Knott (ibid) further showed that an effective surface energy value of 14Jm^{-2} for ferrite satisfied their fracture stress results and a grain size dependence for cleavage fracture stress was demonstrated.

In a tempered pressure vessel steel examined by Curry (89) with a carbide size less than 0.5mm diameter, the critical stress required by the Curry and Knott proposal was greatly in excess of the observed values and it was therefore assumed that a mechanism for cleavage other than the propagation of microcracks in carbide particles was required. It was indicated that the same microstructural features controlled both yielding and cleavage. Kotilainen came to a similar conclusion and proposed this microstructural variable to be the average mesh length of the dislocation network. The Curry and Knott investigation showed that yielding was controlled by grain size, but cleavage by carbide thickness.

If it is assumed that the initiation process is controlled by dislocation phenomena then for the process to be propagation rather than mechanism controlled there must be a dislocation dependent route to easy crack initiation which is related to tensile stress (Stroh 90) . Cottrell (20) proposed a mechanism where dislocations slipping on intersecting {101} planes in bcc metals interact to form sessile dislocations with Burgers vectors perpendicular to the {100} cleavage plane leading to the formation of a wedge shaped crack which can then propagate at the necessary stress level. If the carbide particle cracking route is assumed, slip characteristics are still important since the cracking of brittle particles is a result of applied stresses from dislocation pile ups.

Ritchie, Knott and Rice (91) introduced the concept of a parameter relating fracture toughness to yield stress and fracture stress. This is the characteristic distance, X_0 , over which the fracture stress must be exceeded before cleavage fracture can occur. X_0 is estimated from the stress distribution at the crack tip.

An attempt was made by Malkin and Tetelman (92) to correlate yield strength, cleavage fracture strength and fracture toughness by applying a formula which gives K_{IC} as a function of the notch root radius p :

$$K_{IC}(p) = 2.89 \sigma_Y (\exp [\sigma_{fC}/\sigma_Y - 1] - 1)^{1/2} \sqrt{p}$$

For some materials a limiting value of $p = p_0$ was found below which fracture toughness is independent of p and knowing p_0 a dependence between σ_Y and K_{IC} can be found.

Floreen, Hayden and Devine (93) investigated cleavage initiation in three iron-nickel alloys containing 0.3, 1.9 and 3.9% nickel. It was found that the presence of nickel markedly increased the cleavage fracture strength of the material due to an increased resistance of the ferrite matrix to the growth of micro-cracks from brittle particles. It was suggested that this was a result of some change in the slip characteristics of the ferrite, but it was uncertain as to which deformation parameters were the most critical in the region of cracks and structural defects.



In carbon-manganese weld metal McRobie and Knott (94) found a reduction in toughness with strain aging of both as-deposited and re-heated weld metal. Based on a previous model developed by Tweed and Knott (95) which proposed cleavage fracture initiated by non-metallic inclusions in carbon-manganese weld metal this was explained by the effects of strain aging on material flow. Furthermore, the observation of the variation in size and distance from the crack tip of these inclusions gave an explanation of the degree of scatter to be expected in the study of toughness parameters.

Judson and McKeown (64) described research at Harwell (96) and Cambridge (97) which demonstrated that in ferritic weld metal pro-eutectoid ferrite was the phase that tended to cleave, and also referred to a study by Tweed and Knott (95) which discovered that 1 μ m diameter inclusions were often found at the centre of brittle facets on the fracture surface.

On the basis of this, the proposal was made that dislocation pile-ups inducing cracking of these particles was the mechanism for cleavage initiation. As a result of these investigations a study was made at Harwell of the characteristics of as-deposited ferrite types. Microhardness values were determined for pro-eutectoid, acicular and reheated ferrite and the effect of stress relieving on macro-hardness was also studied. The structure was examined by transmission electron microscopy and no difference was found in dislocation density between as-deposited acicular and pro-eutectoid ferrite.

The dislocation density of all as-deposited material was 3×10^{10} /cm but stress relieved material had much lower values of 1×10^9 to 1×10^{10} /cm . The conclusion was that the observation that cleavage initiated in pro-eutectoid ferrite but was arrested by acicular ferrite was due to a grain size effect. This was confirmed by the observation that the variations in hardness observed were also due to grain size.

Judson and McKeown (64) presented data on nickel additions to manganese containing weld metals which showed that the addition of nickel at levels of around 0.6% manganese improves the resistance of weld metal to cleavage. With an increase of manganese to 1.6% the addition of nickel improves cleavage resistance initially but the effect becomes reversed above 2.4% nickel.

It is the aim of this study to further investigate the interrelationship between nickel and manganese on cleavage in ferritic weld metal and develop possible mechanisms for the results observed by other workers.

3. EXPERIMENTAL METHODS

3.1 Introduction

To determine the effects of manganese and nickel alloying additions on the cleavage behaviour of ferritic weld metal, it is important to examine this behaviour from several viewpoints. This allows an overall picture to be developed which can then be related to the tendencies observed in previous studies. The central element of this research has been the measurement of cleavage strengths by the slow bending of notched testpieces. This has been based on the application of slip line field theory and examines the maximum tensile stress present at the time of cleavage failure. A parallel programme of investigation investigated the fracture mechanics of cleavage for these materials in terms of the critical stress intensity factor in the crack opening mode (K_{Ic}). This parameter describes the critical stress environment for failure at the tip of a theoretically atomically sharp crack.

To allow comparison of these results with the more commonly measured empirical parameters of toughness, notch impact toughness testing was also carried out.

In addition to the mechanical testing described above, further information was obtained by optical and electron microscopy of the fractured material and X-ray analysis of the fracture surfaces.

3.2 Experimental Materials

At the beginning of the investigation two commercially available electrodes supplied by Murex Welding Products (part of the ESAB Group) were used. These were Ferex 7016 and Hi-Trex 7016 C1L.

Ferex 7016 is a carbon-manganese basic electrode conforming to BS639:E5156:B24H and equivalent to AWS type E7016. The manufacturers claim good low temperature as-welded CTOD and Charpy V notch toughnesses coupled with an all-positional capability.

Hi-trex 7016 C1L is a carbon-manganese nickel basic electrode approximately equivalent to BS2493:2N:BH and corresponding to AWS type E7016 C1L. This electrode is claimed to produce weld metal with a controlled tensile strength as well as good Charpy V notch and COD toughness down to -70°C and -51°C respectively. As with Ferex 7016 this electrode has an all-positional capability. Both electrodes have been widely used in offshore fabrication.

The nominal composition of weld metals produced from these electrodes is shown in Table (3.2.1).

In order to expand the range of compositions studied, Murex formulated and produced six experimental electrodes similar to the E7016 type having Mn contents between 0.6 and 1.6% and Ni contents between 0.0 and 2.5%. The nominal compositions of weld metals produced from these electrodes are shown in Table (3.2.1).

Table (3.2.1) Nominal composition of experimental electrodes

WELD	Mn%	Ni%
7016	1.6	0.0
7016C1	0.6	2.6
A	1.0	2.5
C	0.6	1.5
D	1.0	1.5
E	1.6	1.5
F	0.6	0.0
G	1.0	0.0

Mild steel parent plates measuring 300 x 300 x 15 mm and a 5 mm thick mild steel backing bar was used.

3.3 Welding Procedure

To allow a sufficient cross-section of all-weld metal in the test pieces and to ensure that no dilution occurred in the centre line of the weld, a square edge preparation, multi-run, technique was used. A total of 18 runs were made using a semi-buttering welding pattern. The position and sequence of the welding runs is shown in Fig (3.3.1). The welding procedure used was in accordance with BS639 for all-weld metal joints.

Prior to welding, the plate edges were cleaned of any oxide, oil or swarf residues. Previous work had shown that when producing



weldments of this type the results of thermal stressing gave rise to bending of the weldment about the weld line.

In order to counteract this tendency a clamping arrangement was developed which held the plates at a pre-determined angle during welding. Immediately after welding, the plates were released from the jig and on cooling to room temperature were found to be flat. The clamping arrangement is shown in Fig (3.3.1). Without this procedure it would not have been possible to produce the required test piece geometry.

Prior to welding all consumables were re-dried at 150°C for 1 hour (BS5135 Appendix E:Scale C) in accordance with the manufacturer's instructions. Tests carried out by Murex Welding Products Ltd and quoted in product literature have shown that this will give as-deposited hydrogen levels of less than 10mls/100g weld metal under the conditions specified in BS639:1976.

Welding was carried out in the down-hand position with DC electrode positive current. The power source used was a Murex 300 transformer-rectifier. The nominal welding current used was 140A, but this was continuously measured during welding. This was initially carried out using a simple electronic circuit and a chart recorder. Later an OIS weld monitor was purchased which gave a read out of current, voltage and heat input. The interpass interval was also measured. These measures were taken to ensure consistency from run-to-run and plate-to-plate.

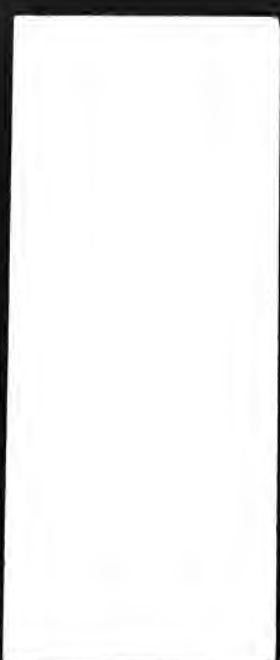
3.4 Test piece preparation

After the completion of welding, the outer edges of the parent plate (ie away from the weld line) were trimmed by flame cutting to give a rough plate width of 150 mm. This was necessary for two reasons; to allow the plates to fit the available machinery and to reduce weight for handling. Immediately after welding the plates were stamped with an identification code corresponding to the manufacturer's batch number.

Using a cold saw, the plate edges were then trimmed and a length removed from the start and finish of the weld. This was to prevent any effects of atypical heating and cooling being reflected in experimental results. Initially 50 mm was removed from each end but it was later found by metallographic examination that a 30 mm off-cut was acceptably conservative and allowed more test pieces to be produced from each plate.

After the plates had been trimmed a lathe was used to turn the plates to the required thickness, leaving a margin for final grinding. Test pieces were then sawn from the prepared plate and ground to the final dimensions. Each test piece was stamped with the plate number and position in the plate starting at the weld start.

Test pieces for both cleavage fracture strength testing and K_{Ic} determination were prepared in accordance with BS5447 for three



point bend testing. The blank test piece dimensions were 13 mm x 26 mm x 120 mm. A slot was milled through the centre of the weld and in the direction of cutting. A special tool was used to machine a 60° V at the bottom of the slot. Test piece geometry is shown in Fig (3.4.1). BS5447 calls for a pre-fatigued crack at the root of the notch when determining K_{Ic} values. This was not necessary for cleavage testing.

Following preparation, all test pieces were stored in a dessicator for at least one week before testing to standardise any possible ageing effects.

3.5 Homogenisation of Microstructure

Although the sample preparation described in 3.4 was adopted for all specimens, the as-welded microstructure is by nature heterogeneous. This is a result of the multi-run welding procedure and leads to the presence of as-deposited material and material which has been re-heated to various degrees. This may result in a considerable degree of scatter in test results since crack initiation will reflect both the metallurgical phases and proportion of such phases sampled at the notch root.

Although mechanical testing of the as-welded material was necessary to provide comparison with standard manufacturer's data and to represent the conditions experienced in real applications, it was felt that the effect of alloying additions on matrix properties could be more readily assessed using a homogenous



structure. For this reason it was decided to produce, through heat treatment, a uniform microstructure typical of re-heated weld-metal. On the basis of published cooling data (98) and experimental experience, a heating cycle was devised which would give an equi-axed grain structure of a size typically found in the re-heated areas of a multi-run weld.

Samples were placed in a tube furnace pre-heated to 1000°C and containing an argon atmosphere. This led to a temperature drop as the furnace was opened and the sample inserted. At this stage it was ensured that the notch of the test piece lay on the centre line of the furnace and that the thermocouple tip lay on the centre line of the specimen. The furnace was then re-sealed and the time taken to regain 1000°C noted. The sample was then held at 1000°C for fifteen minutes.

After this time the furnace tube, still sealed and with argon flowing, was slid out of the heating zone and allowed to cool to 600°C. This time was typically 15 to 20 minutes. To ensure consistency between samples, each was treated separately to ensure a constant thermal mass, the same furnace was used, and the argon flow monitored by visual inspection as it bubbled through a water trap.

In the case of Charpy V notch specimens, heat treatment was carried out on four at a time to give a similar thermal mass in the central zone of the furnace.

3.6 Cryostatic Test Cell

3.6.1 General Requirements

Before any low temperature mechanical testing was possible, it was necessary to adapt the Mayes tensile testing machine for such studies by the construction of a cryostatic test cell. The requirements for this were that it be able to maintain a temperature constant to within 5°C at temperatures down to -170°C. The basic principle decided upon for the cell was that of double-chambered unit cooled by a spray of liquid nitrogen. The inner chamber was to be designed to have good thermal conductivity and a large thermal mass to give temperature stability and the outer chamber was insulated to prevent heat flow into the system.

Design considerations needed to include: access for specimen placement and removal, allowance for the ram movement of the mechanical testing machine, the need to provide connections to the instrumentation contained within the test chamber (ie clip-gauge and thermocouples), rapid assembly and dismantling to allow other users access to the testing machine and low cost.

3.6.2 Inner Chamber

The inner chamber was designed to be fixed to the stationary beam of the testing machine enclosing the upper portion of the three-point bend jaws. The ideal material would have been copper for the best thermal properties but this would have been prone to damage and difficult to source in the dimensions required. As a



good compromise brass was chosen and the main part of the chamber cut from extruded brass tube 160 mm diameter and with a wall thickness of 1.5 mm. This was brazed to a circular brass top plate which fitted tightly round the circular base to the upper bend jaw.

The liquid nitrogen was supplied to the chamber through the side of the chamber near the top plate and passed through several turns of copper tube coiled tightly around the base of the bend jaws before passing into the chamber through a series of holes drilled in the final turn of the copper tube. The first turn of the copper tube was brazed to the top plate and this coupled with the close contact with the bend jaws contributed to the thermal stability of the unit. A panel was cut from the tubular portion of the chamber to make a removable door allowing access from the front of the testing machine.

3.6.3 Outer Chamber

The outer chamber was built of hardboard lined with expanded polystyrene foam. This took the form of a cubic box and was attached to the lower, moving jaws of the testing machine. The front could be removed for access to the inner chamber and also had a cut out to allow electrical connections for thermocouples and the clip gauge to be made. The top of the chamber was closed by a panel which could slide up and down the fixed upper jaw and which rested under its own weight on the bottom of the box.

3.6.4 Liquid Nitrogen Pump

The original aim was to pump the liquid nitrogen using the pressure build up in the Dewar flask, venting this pressure to atmosphere in order to control the flow. This was found to be insufficiently consistent and so an air compressor was used to control the pressure.

A thermostat relay designed for operation up to 250°C was used with the thermocouple connections reversed. This activated the air compressor when a threshold value was reached and thus forced liquid nitrogen into the inner chamber. A second thermocouple was used throughout to give the actual chamber temperature. Both thermocouples were insulated from each other and clamped under the screw-on knife-edges which held the clip gauge. Some problems were initially experienced with ice forming in the delivery system but this was solved by fitting a magnesium perchlorate dryer.

The positive pressure of gas in the chamber due to the nitrogen boiling ensured that cold gas was always flowing out of the chamber and that no warm gas could flow in. In operation the system was found to give constant reproducible chamber temperatures down to $-180^{\circ}\text{C} \pm 2^{\circ}\text{C}$ when no sample was being tested. During actual testing of bend specimen blanks, a temperature rise was noted as the specimen deformed but this was overcome by reducing the ram speed which allowed this heat to be dissipated (see Section 3.7). The cell is shown schematically in Fig (3.6.1).

3.7 Mechanical Test Procedure for Cleavage Fracture Stress Determination

Samples were prepared as described in Sections 3.3 to 3.5. The test piece geometry and testing procedure were based on BS5447 except that no pre-fatigued crack was introduced. Testing was in three-point bend with the upper part of the test jaws comprising a wedge shaped anvil and the bottom part two rollers with centres fixed at 104 mm (ie 4 W where W is the un-notched test piece width equivalent to 26 mm).

Experimental work was carried out using a Mayes Universal Testing Machine Type ESH 5000. This was operated under position control to give a constant ram speed.

3.7.1 Temperature Rise during Testing

During initial trials the ram speed was set at 2 mm/min. It was observed (see Section 3.6.4) that with the onset of plastic deformation preceeding fracture, a temperature rise was caused in the sample whilst the test chamber temperature remained constant. Typical temperature rises noted were 12°C for a starting temperature of -60°C, 9°C for an initial temperature of -90°C and 2°C for -150°C. Thus during the course of the experiment the yield stress is reduced and the toughness increased. This demonstrated that it was not sufficient to maintain a constant test chamber temperature without obtaining feedback from the test piece. This phenomenon has been treated theoretically by Weichert and Schonert (99). Obviously at those temperatures



where general yielding coincides with the initial fracture stress for cleavage, this will be at a minimum. However, to ensure consistency of results across the complete temperature range the ram speed was reduced to 1 mm/min to allow this temperature rise to be more readily dissipated.

3.7.2 Strain Measurement

Strain during bending was measured using a Welwyn Strain Measurement Ltd Type 102 clip gauge which was held between knife edges screwed onto the specimen. The tapped holes in the specimen for the knife edge attachment were as recommended in BS5447. Values of clip gauge opening and load were recorded on an X-Y plotter integral to the Mayes machine. Before each test the clip gauge was calibrated at 1 mm intervals of opening using a vernier calliper and the X axis gain adjusted to allow for an opening of up to 5 mm. A rough zero point was set at room temperature and this was then finally set at the test temperature, thus allowing for the thermal contraction of the test piece.

3.7.3 Load Measurement

Load was measured using the integral load cell within the cross head of the Mayes testing machine. This was displayed digitally and recorded on the X-Y plotter. The maximum scale reading was set at 50 kN.

3.7.4 Cleavage Fracture Stress Calculation

In the bending of SENB specimens a local stress concentration occurs at the notch. Plastic deformation is therefore initially localised at this stress concentration. The stress level at which this plasticity first spreads across the whole cross-section of the test piece is known as the General Yield Stress (σ_{GY}).

Cleavage failure of the specimen will occur when a critical value of tensile stress is achieved either before or coinciding with the onset of general yielding. Thus for a given test piece, geometry and material, there will come a point as the test temperature is decreased where all subsequent failures will be by cleavage. Slip line field theory (83) gives a relationship between the maximum tensile stress σ_{max} , the notch angle θ (in radians) and the shear yield stress of the material τ_y :

$$\sigma_{max} = 2 \tau_y (1 + \pi/2 - \theta/2)$$

This implies that if the tensile yield stress is known the shear yield stress can be calculated and hence the maximum tensile stress at general yield obtained. When, at a given test temperature, general yielding is coincident with the cleavage fracture strength, the calculated value of maximum tensile stress will be equivalent to the cleavage fracture stress at that temperature. Thus, assuming that low enough test temperatures

are used, it should be possible to obtain for each test specimen a cleavage fracture stress at a transition temperature related to the test piece geometry and the material composition.

Since it has been stated (100) that the value of cleavage fracture strength is not strongly dependent on temperature, variations in the transition temperature should not affect the comparison of cleavage fracture stresses from material to material.

3.7.5 General Yield Load Determination

The general yield load was obtained from the load/clip gauge plot by the geometric construction shown in Fig (3.7.5.1). From this, the shear yield stress τ_y at general yielding can be calculated (83) using the formula:

$$\tau_y = \frac{P_{GY}}{0.484 wa}$$

where τ_y is the shear yield stress

P_{GY} is the general yield load

w is the specimen width

d is the notched specimen thickness

3.7.6 Specimen Preservation

It was found that the large degree of condensation and ice formed on the specimen as it warmed up after testing led to a degree of rusting on the fracture surfaces. To overcome this, test pieces

were sprayed with WD40 immediately before and after testing and placed in a dessicator immediately after this.

3.8 Plane Strain Fracture Toughness Testing (K_{Ic})

Initial test piece preparation was as described in Sections 3.3 to 3.5, the test piece geometry being as described in BS5447. Testing procedure was in accordance with that described in Section 3.7 with the additional preparatory operation of introducing a fatigued crack at the root of the notch. In theory, this gives the atomically sharp crack required for the opening mode plane strain fracture toughness (K_{Ic}) to be determined.

3.8.1 Fatigue Pre-Cracking

In order to ensure that no significant plastic deformation is introduced during the pre-cracking stage, BS5447 demands that various restrictions be imposed on the fatigue procedure:

- The fatigue force ratio R should be in the range 0 to 0.1. In practice it was found that to keep the test piece correctly aligned in the jaws of the fatigue machine, the sample was under slight compression even at the stress minimum.
- K_f , the fatigue stress intensity factor, which corresponds to the plane strain stress intensity factor at the

maximum force during the final stage of crack growth, shall not exceed:

$$0.7 \left[\frac{\sigma_{Y1}}{\sigma_{Y2}} \right] K_Q$$

where σ_{Y1} is the 0.2% proof stress at the temperature of fatigue cracking,

σ_{Y2} is the 0.2% proof stress at the fracture toughness test temperature and

K_Q is a provisional value of K_{Ic} before the test validity is established.

This implies that assumptions must be made about the expected values of σ_{Y1} , σ_{Y2} and K_Q before the results of the test are known. At room temperature a conservative estimate of the value of K_{Ic} for this type of material would be approximately $200 \text{ MNm}^{-3/2}$. For the ratio of σ_{Y1}/σ_{Y2} an approximation of 0.5 was assumed.

Thus:

$$K_f \text{ must not exceed } 0.7 \times 0.5 \times 150$$

However, K_f can be calculated as

$$K_f = \frac{P_f Y_1}{B W^{3/2}}$$

where P_f is the fatigue load

Y_1 is a compliance factor determined by the test piece geometry and given in BS5447 for a given ratio of effective

crack length (a) to test piece width (w) (in this case assumed to be 0.5 giving a value of 10.6)

B is the specimen thickness (13 mm)

W is the specimen width (26 mm)

Thus the maximum value for P_f was estimated at:

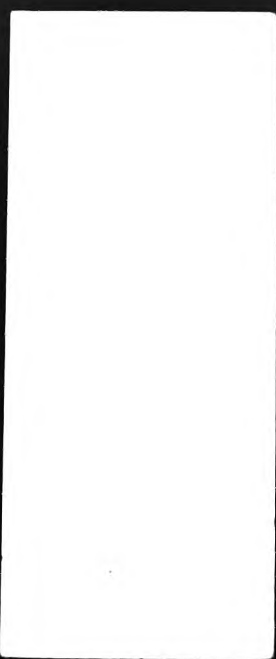
$$0.7 \times 0.5 \times 150 \times 10^6 = \frac{P_f \times 10.6}{(0.013) \times (0.026)^2}$$

ie $P_f \text{ max} = 10.38 \text{ kN}$

In practice it was attempted to keep the value P_f well below this value but at a level where the pre-fatiguing could be carried out in a matter of hours.

- The length of the fatigue crack was specified as being not less than 1.25 mm and such that an a/w ratio (measured after fracture) should be in the range 0.45 to 0.55.
- The crack should fall within a limiting envelope (as shown in Fig (3.8.1.1)).

Fatiguing was carried out using a Datec 200 kW unit at a frequency of approximately 10 cycles per second. Any increase in the fatiguing speed reduced the amplitude set at the beginning of the process. Fatiguing was carried out at room temperature using a specially made 3 point bend jig corresponding in dimensions to



that of the Mayes testing machine. Crack growth was monitored visually using a magnifying lamp. It was however, found by experience that examination using a metallurgical microscope revealed further crack growth and this was taken into consideration. Experiments were made using ultra violet dye penetrant inks but this was found to be more cumbersome than useful. The maximum, minimum and mean stress levels were noted as were the number of cycles.

After pre-fatiguing, samples were placed in a dessicator prior to final testing.

After toughness testing, the fatigue crack was examined to ensure that the criteria specified in BS5447 had been met. These require that the crack length should be measured to the nearest 0.5% x the specimen width at the positions 25%, 50% and 75% of the thickness. If any of the following are the case, the test is deemed invalid:

- The difference between any two of the crack length measurements is greater than 2.5% of the width.
- The difference between the maximum and minimum lengths is greater than 5.0% of the width.
- Any part of the crack part is closer to the machined notch than 2.5% of the width or 1.25 mm whichever is the greater (in this case 1.25 mm).

- any part of the crack surface lies in a plane more than 10° from the plane of the notch.
- the fatigue crack is in more than one plane.

3.8.2 Determination of K_Q

The value of K_Q , the provisional value of K_{Ic} before validity is determined is calculated using the equation:

$$K_Q = \frac{P_Q Y_1}{BW^{3/2}}$$

where P_Q is a force determined by constructing a line through the origin at an angle of 5° to the elastic part of the load/clip gauge opening curve and Y_1 is a compliance factor. P_Q is equivalent to the force where this second line intersects the curve or any higher force preceding this point on the curve.

The standard specifies that the initial slope of this curve should be between 40° and 60°. Since it was desirable to accommodate K_{Ic} and cleavage tests on the same scale, this was not however possible and the slope was therefore approximately 80°. Obviously this does not affect the test conditions but merely the graphic display of the results.

Validity criteria arising from the test results are:

- The deviation at $0.8P_Q$ from the linear should be less than 0.25 that at P_Q .

The final checks on the validity of the original assumptions are that:

- Neither crack length or thickness exceed $2.5 (K_Q/\sigma_Y)^{1/2}$
- K_f does not exceed $0.7 K_{IC}$

3.9 Tensile Testing

Although tensile yield strengths can be calculated by applying Tresca or Von Mises yielding criteria to the formula of Green and Hundy, it was thought desirable to cross check this experimentally. A cryostatic tensile test rig was designed to fit on an Instron tensile testing machine.

This used a Hounsfield Tensometer type test piece machined from the test plates across the weld and designed so that the gauge length was all weld metal. The cell consisted of a perspex cylinder which fitted tightly over a rubber bung on the lower jaws of the testing machine. This allowed a mixture of Propan-1-ol and liquid nitrogen to be poured into the perspex cylinder and surround the test piece. The cylinder was insulated with expanded polystyrene and the temperature of the cryogenic liquid monitored using a thermocouple. The test rig could however only achieve test temperatures down to -80°C .

Since the only bend tests carried out at this temperature revealed fully ductile failure the comparison with the tensile test pieces served no useful purpose. There was, additionally, only a limited amount of as-welded material remaining and it was felt that further work to refine the technique could not be justified.

3.10 Impact testing of weld metal samples

To complete the programme of mechanical testing Charpy 'V'-notch impact measurements were made on all the as welded and re-heated weld metals. To allow comparison with cleavage fracture stress and fracture toughness measurements these were carried out at -150°C .

Samples were prepared in accordance with the British standard with the notch in the direction of welding. Heat treatments were carried out as for the bend specimens with four specimens placed in the furnace at one time to give a comparable thermal mass and similar cooling characteristics.

Before testing a thermocouple was attached to the specimen which was then immersed in a bath of liquid nitrogen for 20 minutes. The sample was then removed from the liquid nitrogen and placed on the Charpy machine. When the temperature reading from the thermocouple reached -150°C the striker was released and the



energy absorbed during the fracture of the specimen noted. Observation showed that the temperature rise during the testing was too small to be measured.

3.11 Electron microscopy

All fracture surfaces were examined in a scanning electron microscope at a variety of magnifications appropriate to the surface features. Where possible cleavage initiation sites were identified and photographs taken in order to characterise the initiator. A general view of the fracture surface was also photographed.

3.12 Optical microscopy

Weld metal microstructures were examined at various magnifications. Samples were sectioned parallel to the fracture face, polished down to one micron and etched in 5% Nital at room temperature. Grain sizes were determined from photo-micrographs using a linear intercept method. Magnifications were verified by including in each set of photographs one shot of a calibrated gauge length. At the macroscopic level unsuccessful attempts were made to reveal the degree of plastic deformation using Fry's reagent.

3.13 Chemical analysis

Chemical analyses were carried out by Murex Welding Products Ltd.

4. EXPERIMENTAL RESULTS

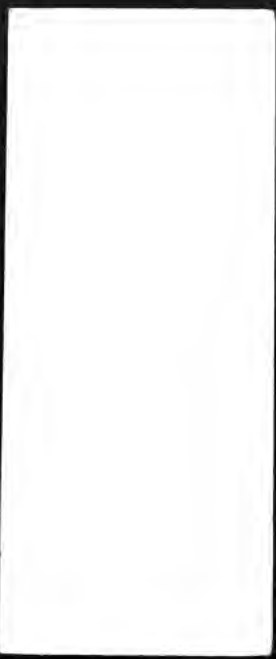
4.1 Consistency of welds

The first series of experimental welds was prepared using a simple monitoring circuit recording time and welding current. This showed consistency from run to run and weld to weld, but could not be taken as truly quantitative. For the final two test plates of 7016 and 7016C1 an OIS PAMS II weld monitor was available which sampled weld current and voltage at two second intervals and gave average values for each run as well as time elapsed and total arc energy. As the weld procedure was otherwise unchanged it is reasonable to assume that similar conditions prevailed in the earlier test plates.

Assuming the actual weld length on the 300mm plates was of the order of 270mm an approximate arc energy of 0.8kJ/mm was obtained.

4.2 Consistency of heat treatment

Heat treatments were carried out in batches of a single weld metal composition in an inert atmosphere tube furnace. After 15 minutes at the austenitising temperature of 1000°C cooling curves were measured with readings at one minute intervals down to 600°C. The samples were then allowed to cool in air to room temperature. It is interesting to note that on exposure to air temper colours were produced on the samples which clearly showed



the position of the individual weld runs. This is perhaps a very subtle indication of segregation although considering the microscopic differences in oxide thickness required to give a change in colour it is difficult to draw any further conclusions from this. Cooling curves are shown in Fig 4.2.1.

4.3 Microstructure and grain size of re-heated weld metal

The microstructures obtained by using the heat treatment cycles described in section 4.2 proved, as far as could be ascertained, to be identical to those found in the re-heated portions of as-welded deposits of similar compositions. As opposed to the results found by King (101) there was no pronounced scatter in grain sizes although it should be noted that the sample sizes here were somewhat smaller.

The microstructure for each composition was broadly similar comprising equiaxed, fairly regular ferrite grains with intergranular areas of pearlite. The pearlite was often present in bands suggesting continuing micro-segregation resulting from the previous as-deposited structure. The ferrite grain sizes measured for each composition as well as Standard Deviations are shown in Table 4.3.1.

Table 4.3.1 Ferrite grain sizes for re-heated weld metal

Composition	Grain size(mm)	S.D ($\times 10^{-3}$)
7016	0.017	1.53
7016C1	0.015	3.09
A	0.01	0.425
C	0.014	0.695
D	0.014	0.818
E	0.012	1.08
F	0.017	1.87
G	0.013	0.824

Photo-micrographs of the re-heated weld metal samples are shown in Figures 4.3.1 to 4.3.8. The samples can be ranked in order of decreasing grain size as shown below:

7016 > F > 7016C1 > C,D > G > E > A

This ranking order seems to show a possible correlation with general yield strength in some cases but with exceptions that make it appear that this is mere coincidence and that the grain size effect is in this case a minor consideration. (See Section 4.5.2.3). The correlation between grain size and mechanical properties appears to break down when cleavage fracture strength is considered. (See Section 4.5.2.5)

4.4 Chemical Analysis

Chemical analysis of the experimental electrodes was carried out by Murex Welding Products Ltd of Waltham Cross, part of the ESAB Group. The compositions found, which are shown in Table 4.4.1 below show fairly good agreement between the nominal and actual values for manganese and nickel. Carbon equivalents were also calculated using the formula:

$$CE = C + \frac{Mn + Si}{6} + \frac{Ni}{15}$$

Table 4.4.1 Nominal and actual manganese and nickel compositions

WELD	NOMINAL		ACTUAL				CE
	Mn%	Ni%	Mn%	Ni%	Si%	C%	
7016	1.6	0.0	1.9	0.03	0.45	0.061	0.45
7016C1	0.6	2.6	0.66	2.52	0.37	0.060	0.4
A	1.0	2.5	1.0	2.7	0.46	0.056	0.48
C	0.6	1.5	0.72	1.69	0.36	0.060	0.35
D	1.0	1.5	0.99	1.7	0.45	0.057	0.41
E	1.6	1.5	1.67	1.58	0.5	0.055	0.52
F	0.6	0.0	0.75	0.02	0.41	0.063	0.25
G	1.0	0.0	1.03	0.02	0.48	0.063	0.32

4.5 Mechanical Testing

4.5.1 Notched Bend Testing of As-Welded Samples

Several measurements can be taken from the load versus clip gauge opening curves, the typical form for which is shown in Fig(4.5.1.1) .It can be seen that the curves take the form of elastic extension followed by yielding, plastic deformation and work hardening to fracture.

General yield loads can be obtained by extrapolating the elastic and plastic portions of the curve (point GY on Fig 4.5.1.1).Fracture loads can be measured directly from the graph.The amount of plastic deformation can give an indication of toughness at a given temperature for that sample configuration using the offset method shown in Fig(4.5.1.2)

The first series of mechanical tests carried out were slow bend tests on notched as-welded samples of 7016 and 7016 C1.The test temperatures for this initial work were chosen as -60°C , -90°C , -150°C , -120°C , -135°C and -150°C .The general yield load, fracture load and plastic strain for each composition at each temperature are shown in Table 4.5.1.1.

Table 4.5.1.1 General yield load, fracture load and plastic strain for as-welded 7016 and 7016C1

ELECTRODE	T°C	PGY (kN)	PF (kN)	d plastic mm
7016	RT	23.3	-	-
	-60	24.8	29.5	-
	-90	26.0	30.5	-
	-105	26.7	32.0	2.47
	-120	27.4	31.0	1.44
	-135	29.3	31.0	0.70
	-150	29.9	29.9	0.46

ELECTRODE	T°C	PGY (kN)	PF (kN)	d plastic mm
7016C1	RT	21.6	-	-
	-60	25.0	30.5	4.89
	-90	25.3	30.5	4.45
	-105	26.0	32.0	3.95
	-120	25.6	30.6	2.00
	-135	27.3	33.5	3.75
	-150	27.7	29.8	0.45

It can be seen that at the higher temperatures a considerable degree of plastic deformation occurred for both compositions.



indeed for 7016 at temperatures above -150°C the plastic crack opening was greater than the clip gauge could measure. As expected the degree of plastic deformation generally decreased with temperature although there was some scatter and the occasional anomalous result.

General yield loads for both 7016 C1 were comparable with but slightly lower than those for 7016 and increased with decreasing temperature. Despite the slightly reduced general yield loads for 7016 the fracture loads were similar for the two compositions indicating a higher degree of yielding before fracture for 7016 C1. It should be noted that in neither of these test series on as-welded material were Lüders strains evident.

Only in the case of 7016 was the temperature sufficiently depressed to allow fracture to coincide with general yielding thus enabling a calculation of cleavage fracture strength to be made. For 7016 C1 an estimated figure was obtained. The values of cleavage fracture stress for all compositions are discussed in Section 4.6.2.5

4.5.2 Notched Bend Testing of Heat Treated Samples

4.5.2.1 7016 and 7016 C1

When the slow bend tests were repeated on heat treated material the temperature testing range was amended to -60°C to -170°C in an attempt to ensure that cleavage values could be obtained. Yield

loads, fracture loads and plastic deformation before fracture for re-heated 7016 and 7016 C1 are shown in Table 4.5.2.1.1.

Table 4.5.2.1.1 Yield loads, fracture loads and plastic deformation for re-heated 7016 and 7016C1

ELECTRODE	T°C	PGY (kN)	PF (kN)	d plastic mm
7016	-60	15.6	-	-
	-130	19.7	23.2	1.88
	-150	21.3	23.5	1.46
	-170	25.9	25.9	0.18

ELECTRODE	T°C	PGY (kN)	PF (kN)	d plastic mm
7016C1	-60	17.6	-	-
	-130	20.4	25.6	2.32
	-150	23.2	23.5	0.66
	-170	26.0	26.0	0.156

The most obvious difference between the two test series is that the clip gauge/load curves for re-heated material showed the presence of Lüders strains which broadly increased with decreasing temperature.

General yield loads and fracture loads were considerably lower

than for the as-welded samples. Fracture loads for the two were comparable, but as opposed to the as-welded material, yielding loads were slightly lower for 7016.

In both cases fracture coincided with general yield at -170°C allowing cleavage fracture strength to be calculated.

4.5.2.2 Experimental electrodes A,C,D,E,F,G.

The experimental electrodes A,C,D,E,F,G were only tested in the heat treated condition. On the basis of the experience with the previous test series the test temperatures chosen were -130°C , -150°C and -170° . The curves produced for load/clip gauge extension followed the same pattern as for the reheated samples of 7016 and 7017C1 with elastic extension followed by plastic deformation and fracture or fracture at general yielding. Of the six experimental electrodes only four namely C,D,F and G showed Lüders strains. The general yield loads, fracture loads and plastic deformations for each composition at each temperature are shown in Table 4.5.2.2.1.

Table 4.5.2.2.1 General yield loads, fracture loads and plastic deformation for re-heated experimental electrodes

ELECTRODE	T°C	PGY (kN)	PF (kN)	d plastic mm
A	-130	20.5	24.5	0.85
	-150	22.5	25.5	0.62
	-170	24.0	25.6	0.24

ELECTRODE	T°C	PGY (kN)	PF (kN)	d plastic mm
C	-130	22.5	22.5	2.07
	-150	23.6	25.0	1.57
	-170	25.6	25.6	0.78

ELECTRODE	T°C	PGY (kN)	PF (kN)	d plastic mm
D	-130	21.6	27.0	2.28
	-150	23.0	26.0	1.5
	-170	26.5	27.2	0.77

ELECTRODE	T°C	PGY (kN)	PF (kN)	d plastic mm
E	-110	19.0	26.2	0.49
	-130	18.5	22.0	0.29
	-150	16.8	16.8	0
	-170	15.0	15.0	0



ELECTRODE	T°C	PGY (kN)	PF (kN)	d plastic mm
F	-130	20.0	21.7	1.97
	-150	23.5	23.5	0.61
	-170	24.5	24.5	0.1

ELECTRODE	T°C	PGY (kN)	PF (kN)	d plastic mm
G	-130	21.7	29.5	4.59
	-150	25.6	25.6	0.32
	-170	26.7	26.7	0.29

4.5.2.3. Comparison of general yield loads for re-heated material

Viewed as a whole it is clear that for all compositions the value of general yield load increases with decreasing temperature as would be expected. Comparing the temperature dependence of the general yield stress for each composition it can be seen that this is of a similar form for each. The only apparent exception to this is experimental composition E, however it should be borne in mind that only at the exceptionally high test temperature of -110°C did general yielding occur before fracture and at the test temperatures below this fracture by cleavage occurred before or coincident with yielding.

For samples F and G it should also be noted that fracture coincided with general yielding at -150°C therefore values for general yielding at -170°C are not applicable. Thus if the test temperature of -130°C is chosen at which to compare general yield strengths for each composition (and taking into account that no such value is available for composition E) the yield strengths for the various compositions can be ranked:

C > G, D > A, 7016 C1 > F, 7016

(commas indicate a value only slightly greater than)

Looking at Figures 4.5.2.3.1. to 4.5.2.3.7 which group electrodes with similar manganese and nickel values and rank them in the order shown above several observations can be made.



Compositions G,D and A ,each with 1.0% manganese show a decrease in general yield strength with increasing nickel.Compositions E and 7016 with 1.6% manganese appear to show a similar trend.Compositions C and 7016C1 with 0.6% manganese + nickel would also appear to follow a similar pattern although for composition F with 0.6% manganese and no nickel this is not the case.Compositions C,D and E with a constant nickel content of 1.5% show a decrease in general yield strength at -130°C with increasing manganese.Compositions G,F and 7016 with no nickel indicate an optimum value of 1.0% manganese.Compositions A and 7016C1 with 2.6 and 2.5% nickel respectively suggest a strengthening effect with increased manganese.

These apparent trends show that both manganese and nickel play a role in the processes which determine general yield strength although exactly what role is not necessarily clear.Contrary to the effect which might be expected from simple solid solution strengthening the two elements when combined seem,under these conditions ,to decrease strength with increased concentration.

1.5.2.4. Comparison of fracture loads for re-heated material.

Comparison of fracture loads for these materials is complicated by the different failure modes operating i.e. yielding followed by work hardening and fracture,general yielding and fracture coincident and fracture before general yielding.Fracture loads will therefore only be discussed in terms of cleavage by comparisons of cleavage fracture strengths.

4.5.2.5 Comparisons of cleavage fracture strength

The cleavage fracture strength for each composition was determined from the shear yield strength at the temperature where fracture first coincided with general yielding using the formula:

$$\sigma_{\max} = 2\tau_y (1 + \pi/2 - \theta/2)$$

The general yield shear stresses were calculated from the general yield loads using the formula:

$$\tau_y = \frac{P_{GY}}{0.484 wa}$$

(the terms in these formulae are introduced in section 3.7.4)

The values obtained for each composition and the temperatures at which they were achieved are shown in Table 4.5.2.5.1

Table 4.5.2.5.1 Cleavage fracture stresses, general yield shear stresses and temperatures where general yielding was coincident with fracture

ELECTRODE	σ_{max} ($\times 10^8 N/m^2$)	τ_{GY} ($\times 10^8 N/m^2$)	T°C
7016 (as welded)	12.16	2.97	-150
7016C1 (as welded)	(12.12)	-	<-150
7016	10.52	2.57	-170
7016C1	10.56	2.58	-170
A	(10.4)	-	<-170
C	10.4	2.54	-170
D	11.5	2.7	-170
E	6.83	1.67	-150
F	9.54	2.33	-150
G	10.4	2.54	-150



Cleavage fracture stress values could not be obtained for the as-welded 7016C1 electrodes or for reheated experimental electrode A since fracture did not coincide with general yielding within the temperature range available i.e. down to -170°C.

The value for experimental electrode D is included since, even though coincidence of fracture and general yield did not occur within the temperature range the value at -170°C was within 0.7kN which was considered close enough to give a usable result.

At -170°C the fracture load for A was still 1.6 kN higher than the general yield load of 24kN. However since the fracture load of 25.6kN remained almost constant over both the 150°C and -170°C tests an approximate placing based on this load is included in brackets.

Comparing these figures the ranking in order of decreasing cleavage fracture strength shown below can be obtained:

D > 7016, 7016C1 > C, (A), G > F > E
(all for re-heated weld metal)

Comparing the values for cleavage fracture strength for electrodes with similar manganese and nickel levels (Fig 4.5.2.5.1) the following observations can be made:

For electrodes 7016, F and G, each with no nickel present the cleavage fracture strength increases with increasing manganese.

For compositions C,D and E with 1.5% nickel the highest value is obtained for D with 1.0% manganese.

For compositions 7016C1 and A (bearing in mind the limitations of the result for A) with 2.6 and 2.5% nickel respectively there is a slight decrease in cleavage fracture strength when manganese is increased from 0.6% to 1.0%.

For compositions 7016C1,C and F cleavage fracture strength increases with increasing nickel.

For compositions A,D and G a maximum value of cleavage fracture strength is obtained with 1.5% nickel.

For compositions 7016 and E each with 1.5% manganese the cleavage fracture strength is much lower with 1.5% nickel than with no nickel.

To summarise these results:

■ Both manganese and nickel when not combined improve cleavage strength with increasing additions within the range of compositions studied.

■ In combination manganese and nickel improve cleavage fracture strength with increasing additions up to a level of 1.0% and 1.5% respectively. Beyond these levels further additions of manganese appear to have a detrimental effect and further additions of nickel have little or no effect.

The examination of variation in cleavage fracture strength with carbon equivalent did not reveal any meaningful trends.

4.5.2.6 Effect of alloying additions on temperature at which coincidence of fracture and general yielding occurred.

A comparison of the temperatures at which general yielding and fracture first coincide shows no clear pattern with changing nickel content but does seem to show a certain correlation with manganese contents. Alloys with 1.6% manganese tend to be at the lower temperature end of the scale with coincidence occurring at -150° and -170°C . Three out of four of the compositions with 0.6% manganese show this transition at -170° and two out of three of the compositions with 1.0% manganese show this transition at temperatures below -170°C .

4.5.3 Plane strain fracture toughness testing of re-heated samples

Valid K_{IC} values were obtained for six of the eight re-heated electrode compositions. Sample E twice broke during pre-fatiguing using up all available samples and the value obtained for sample G was found to be invalid, falling outside the test criteria, so that only a K_Q value could be obtained. All plane strain fracture toughness testing was carried out at -150°C . The values obtained for each composition are shown in Table 4.5.3.1 below.

Table 4.5.3.1 Plane strain fracture toughness of reheated samples

Composition	K_{IC} ($\text{MNm}^{-3/2}$)
7016	63.8
7016C1	62.5
A	56.3
C	57.5
D	73.1
E	----
F	63.3
G	(79.4) K_Q only - not valid

From these results the values for plane strain fracture toughness can be ranked according to composition as follows:

D >> 7016 > F > 7016C1 >> C > A

It is also possible to assign a notional position for experimental electrode E as the composition with the lowest fracture toughness as this failed in fatigue under the same conditions as the others were pre-fatigued. It is open to debate how much value can be assigned to this notional placing but it is in line with its rankings for yield strength and cleavage fracture strength.

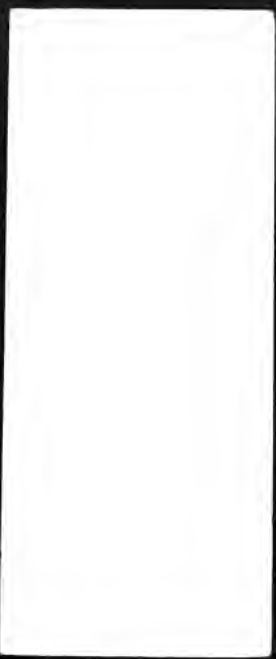
Considering firstly the various manganese regimes:

Compositions F , 7016C1 and C each with 0.6% manganese and 0.0 , 2.5 and 1.5% nickel respectively show no clear pattern, indeed an increase in nickel content from 0.0 to 2.5% gives an almost identical fracture toughness.

For compositions D and A with 1% manganese the fracture toughness is greatly increased when the nickel content is reduced from 2.5% to 1.5%.

For compositions 7016 and E with 1.6% Mn , then if the previous assumption is valid fracture toughness is much better with no nickel than with 2.5%.

Considering now the various nickel regimes:



For compositions 7016 and F with no nickel there is almost no change in fracture toughness when manganese is increased from 0.6% to 1.6% .

For compositions C , D and E with 1.0% nickel an increase from 0.6% manganese to 1.0% manganese gives a dramatic increase in fracture toughness,with D giving the highest value of all the compositions.However, a further increase in manganese to 1.6% again has a dramatic effect,only giving now the lowest fracture toughness.

For compositions A and 7016C1 , each with approximately 2.5% nickel an increase in manganese from 0.6% to 1.0% leads to a decrease in fracture toughness.

Although the combined effects of manganese and nickel at first seem to produce a very confusing pattern some conclusions may be drawn.

- An optimum combination of manganese and nickel exists,namely 1.0% manganese and 1.5% nickel.
- If too much nickel is present then the less manganese the better and if too much manganese is present then the less nickel the better.
- If insufficient manganese is present then even increasing the



nickel from 0.0 to 2.5% does not appear to make much difference.

- If too little nickel is present (or even none at all) then there is little change with increasing manganese.

4.6 Electron microscopy

Scanning electron microscope studies were made of the fracture surfaces for each of the as-welded and re-heated samples. For the re-heated electrodes the surfaces were examined at a range of decreasing fracture temperatures from -105 to -150°C. This showed the transition from mainly ductile to cleavage behaviour but did not give any particular information about the cleavage process and so all comparisons of fracture surfaces for the different compositions of reheated weld metal were made at -150°C fracture temperature.

4.6.1 Comparison of fracture surfaces for as-welded 7016 and 7016C1

Figure (4.6.1.1) shows the area just below the base of the notch for a sample of as-welded 7016 fractured at -105°C. It is clear from the picture which was taken at a 2000x magnification that fracture at this stage was completely ductile with microvoid coalescence the fracture mechanism.

Moving further away from the notch, Fig (4.6.1.2), bands of cleavage fracture showing possible initiation sites begin to



appear. The cleavage surface does not appear particularly faceted but river markings are visible as is an area in the centre left of the picture where cleavage appears to have been initiated either at an inclusion particle or a grain boundary. One area, Fig (4.6.1.3) shows a large slag particle which has fractured in a brittle manner but not initiated cleavage in the surrounding material.

With decreasing temperature the amount of ductile fracture surface and the relative amount of ductile material in the cleavage initiation area begin to decrease. At -120°C the fracture surface again reveals a banded texture with the bands running parallel to the notch root although this is at right angles to any texture which might result from the multi-run weld.

In the suspected initiation area strings of ductile material occur between noticeably 'blocky' cleavage facets, in Fig (4.6.1.4) this structure is particularly dramatic with three mutually perpendicular fracture planes evident in the centre of the picture and indications of an initiation point at the top of this region. Dark circular spots are visible on the cleavage facets which appear to be the site of inclusions which have been ripped out during fracture. Some of these appear to be associated with cracks.

The fracture appearance is similar at -135°C with the amount of ductility further reduced and finally at -150°C the mixed



ductile/cleavage zone is restricted to the notch root and the transition to fully brittle is quite sharp. The dark spots are still visible but so too are light coloured spherical particles. These may be inclusions which have not been completely removed during fracture and in some cases eg Figs (4.6.1.5/6) appear to be associated with cleavage initiation.

The general type of fracture surface observed and the variation with temperature is very similar for samples of as welded 7016C1. Again at lower temperatures the amount of ductile fracture reduces until at -150°C it is present only at the notch root. The fracture surface at -150°C shows an abrupt transition to cleavage just below the notch root with the same dark spots and light spherical particles as were seen with 7016. The cleavage surface is perhaps less heavily faceted than with 7016 and in several cases ,eg Fig (4.6.1.7) it appears that smaller grains have been split in half showing dark spots within and apparent river markings radiating from the spots.

In general there are few differences between the fracture surfaces for the two as-welded materials. If anything the 7016C1 material shows slightly less ductility. Samples of 7016 C1 appear to have more possible inclusions and a more coarse cleavage facet structure but there is a large degree of variation both from sample to sample and within each sample so this is merely subjective conjecture.

4.6.2 Comparison of as-welded and re-heated 7016 and 7016C1

fracture surfaces

The re-heated samples both show a more clearly defined transition zone and less ductile fracture than the as-welded samples. Possible initiation sites appear to be more clearly defined and occur just below the notch root. There appear to be less of the previously observed black spots and more river markings. Figures (4.6.2.1) and (4.6.2.2) show cleavage initiation sites just below the notch root for 7016 and 7016C1 respectively. To the left of centre of Fig (4.6.2.2) is one particularly distinctive site where the initiator appears to be a small grain which has split in half leaving a light coloured disk.

4.6.3 Fracture surfaces of re-heated experimental electrodes

Composition A showed very little ductility and a fairly fine cleavage facet structure. Quite a few light coloured inclusions were visible. A typical area of the fracture surface is shown in Fig(4.6.3.1).

Composition C was very similar in all respects to A, Fig (4.6.3.2), while samples of composition D still showed noticeable areas of ductility, quite large cleavage facets and few black spots, Fig (4.6.3.3).

Composition E showed quite closely spaced river markings and



almost no ductility and a fairly coarse facet structure ,Fig (4.6.3.3).

F showed little ductility numerous river markings,quite a large facet size and few inclusions, Fig (4.6.3.4).

Finally composition G showed a coarse almost scaly facet structure ,noticeable though not large areas of ductility, significant numbers of light coloured inclusions and few black spots.

To summarise the observations made on the re-heated experimental compositions:

- The observed ductility is in accordance with the results of mechanical testing.
- The light coloured spherical particles are almost certainly inclusions and the dark spots show the position of inclusions which have been removed during fracture.
- These inclusions appear to play a role in cleavage initiation and the ratio of inclusions remaining to those lost may also be of significance.
- Further indications as to the progress of the cleavage process may possibly be given by the cleavage facet size and the number and density of river markings.

5. DISCUSSION AND CONCLUSIONS

5.1 Grain size effects and general yielding

In order to enable the effects of alloying on cleavage fracture strength to be judged independently of the complications inherent in an as-welded microstructure all compositions were subjected to an austenitising heat treatment followed by controlled cooling. Since one of the effects of alloying is to change the transformation characteristics of the material this may result in a variation in grain size from composition to composition. It might therefore be argued that the variation in general yield stress from sample to sample is the result of a Hall Petch type relationship. The variation in grain size between the samples was not of the order where it might be expected to have any great effect on samples of the same composition but the lattice friction stress σ_0 and the constant k would of course also change with composition.

Comparing the samples in increasing order of grain size and decreasing order of general yield stress at -150°C we get the following rankings:

Grain size $A < E < G < D , C < 7016C1 < F < 7016$

General yield stress $C > G , D > A , 7016C1 > F > 7016 > (E)$

(The position for the general yield stress of E is included in

brackets since it did not show any ductility at -150°C)

On the basis of these comparisons there does appear to be a correlation for some of the compositions. The two most notable deviations from any correlation are compositions A and E. Both A and E have a lower general yield stress at -150°C than would be expected from a straightforward grain size effect.

There are several possible reasons for this deviation:

- Solid solution strengthening effects
- Microstructural effects
- Effects on the temperature dependence of σ_{GY} with alloying
- Other effects of manganese and nickel on the slip characteristics of the material.

If this variation was the effect of a simple additive solid solution strengthening effects then we would expect compositions with a similar content of one alloying addition but more of the other to show a higher general yield stress at the same temperature.

On this basis it might be expected that A with 1% manganese and



2.5% nickel would have a higher general yield stress than either D or G ,each with 1% manganese but 1.5% nickel and no nickel respectively.

Similarly we would expect E with 1.6% manganese and 1.5% nickel to have a higher general yield stress than 7016 with 1.6% manganese and no nickel respectively.

Since neither of these is the case then if this deviation is the result of variations due to solid solution strengthening then the interaction of the alloying agents must be of a complex nature.

Comparison of the nominal and actual chemical compositions does not show any great discrepancy and it can therefore be concluded that these variations are not the result of poor quality control.

There was no evidence during optical microscopy of any variation between the various samples other than in the grain sizes and so this ,again, seems to be an unlikely cause for depressed yield points for A and E.

Electron microscopy of the fracture surfaces for the two compositions showed no great dissimilarity between these compositions and the others except in the degree of ductility and ,in the case of E, the nature of the cleavage facet structure which was noticeably coarse (although this was no coarser than G which showed a higher general yield strength).



A possible cause for the differences between the yield stresses expected due to grain size effects and those observed is therefore the change in the temperature dependence of the yield strength with alloying. Composition A did not show coincidence of general yielding with fracture even at the lowest test temperature of -170°C whereas composition E showed this at -130°C . All of the other compositions in the re-heated condition showed this coincidence at -130°C or -150°C . Although the variations for A and E are at the opposite extremes of this temperature spread an investigation of the effects of alloying on the temperature dependence of yielding for these compositions might provide at least a partial answer.

Leaving these two compositions to one side it does however seem likely that the grain size effect is at least an important contributor to the variation in yield strength from composition to composition but is not in itself the complete explanation. The effects of alloying on the general yield strengths of the various weld metals will be discussed further in section 5.5.

5.2 The effects of alloying on grain size

If the alloying agents are having a grain refining effect this is in accord with the results observed in previous work including for example Evans (14 - 18) and Taylor and Evans (37).

This effect may either be a result of the alloying on the wrought

equivalent of the weld metal , in other words an equilibrium effect, or may result from the action of these elements on reheated material where the previous as-welded history of the metal is also a factor. If the experimental compositions are ranked in order of carbon equivalent then if this effect is fundamental to the material it might be expected that there would be a correlation between grain size and carbon equivalent.

In order of carbon equivalent the experimental electrodes are:

E > A > 7016 > D > 7016C1 > C > G > F

This does not appear to bear any similarity to the rankings of the compositions in order of either grain size or yield stress.

Since the experimental compositions all underwent a similar heat treatment regardless of their transformation temperatures it might therefore be revealing to calculate how their transformation characteristics relate to the heat treatment of austenitising at 1000°C followed by slow cooling.

Using the formulae of Atkins (98) shown below the A_{C1} and A_{C3} temperatures were calculated for each electrode based on the actual rather than the nominal compositions:

$$A_{C1} (^{\circ}\text{C}) = 723 - 20.7 \text{ Mn} - 16.9 \text{ Ni} + 29.1 \text{ Si}$$

$$A_{C3} (^{\circ}\text{C}) = 910 - 203 \sqrt{\text{C}} - 15.2 \text{ Ni} + 44.7 \text{ Si}$$

These values are shown in Table 5.2.1

Table 5.2.1 Calculated transformation temperatures for experimental compositions

ELECTRODE	A_{C1} ($^{\circ}C$)	A_{C3} ($^{\circ}C$)
7016	696	879.5
7016C1	677.5	838.5
A	670	841.5
C	690	850
D	690	859
E	676	860
F	722.5	877
G	715	880

Since grain growth is a function of time and temperature then it might be supposed that those compositions with the highest A_{C3} temperatures and the lowest A_{C1} temperatures would have the largest grain sizes. In practice the effect of temperature is more likely to be important than the time differences between A_{C3} and A_{C1} under the heat treatment conditions used here.

Continuing this argument that the time factor is less important then a useful comparison would simply be between the A_{C3} temperatures for each composition and the grain sizes obtained. If the samples are ranked in order of increasing A_{C3} then this

should correlate to increasing grain size. The compositions in order of increasing A_{C3} are:

7016C1 < A < C < D < E < F < 7016 < G

It can be seen that there is no correlation between this and observed grain size.

Similar rankings for decreasing A_{C1} and increasing $A_{C3} - A_{C1}$ give:

A_{C1} F > G > 7016 > C, D > 7016C1 > E > A

$A_{C3} - A_{C1}$ F < C < 7016C1 < G < D < A < 7016 < E

Again there appears to be no correlation between these and grain size.

The conclusion which can be drawn from these results is that the grain sizes observed must depend on the effects of alloying on the as-deposited material which then affect the behaviour of the metal on re-heating. This is probably the result of the distribution of inclusions in the as-welded microstructure which pin the austenite grain boundaries on re-heating.

It might therefore be expected that those compositions which give either a high proportion of phases with a small packet size, such as acicular ferrite, or an overall fine grain structure will also give a fine re-heated structure. The role of inclusions as

nucleation sites for ferrite has been reviewed by Pargeter(34) and Devillers et al (35) and from this work it can be concluded that a fine dispersion of inclusions will give a fine ferrite microstructure.

Since in the weld metal the phases present are not the result of equilibrium cooling it is clear that reference to equilibrium transformation temperatures will not be valid. The effects of alloying on weld metal microstructure have been examined in section 2.2.1. Manganese has been shown to increase the proportion of acicular ferrite and refine reheated material and it is claimed that nickel refines the acicular ferrite structure by depressing the transformation temperature (37). This is also said to give a refined re-heated structure. In combination however above certain contents of manganese and nickel the formation of other coarser phases occurs and so it might be expected that a coarser re-heated structure would also result.

From the above it can be concluded that the grain sizes resulting from the heat treatment of these samples can not be ascribed to any simple cause and are the result of an interplay between several factors. These could include the effects of alloying on transformation temperatures, the grain sizes and phases present in the as-deposited weld metal and the distribution of inclusions.

5.3 Lüders strains



As was noted in sections 4.5.2.1 and 4.5.2.2 the majority of the reheated weld metals showed a Lüders strain during low temperature bend testing. This was seen to increase with decreasing temperature but was curtailed by the onset of cleavage fracture although in some instances it was observable at the coincidence of general yielding with cleavage fracture. It is of great interest to note that the two re-heated compositions which did not show any evidence of Lüders strains were A and E, the two compositions where there was a significant deviation from the general yield strength/grain size correlation.

Since Lüders strain represents pure plastic behaviour then if it is observed the presence of mobile dislocations throughout the matrix can be deduced. These become locked as the band of plastic flow passes through the material. The amount of Lüders strain therefore gives an indication of factors affecting the slip characteristics of the material.

If there are in the matrix features which tend to pin dislocations then it might be expected that Lüders strains would be reduced or eliminated. If the presence of alloying agents produces conditions where say carbon and nitrogen segregation is affected this might promote the pinning of dislocations.

Accepting that the change in temperature dependence of yield stress with alloying is an important factor for the sake of comparison the amount of Lüders strain for each composition at 130°C was:

C > G > F > 7016 > 7016C1 > D > (A,E)

This shows a rough correlation to the carbon equivalents for each composition.

5.4 Differences between general yielding of as welded material and re-heated material

As can be seen from Table 4.5.1.1 the general yield and fracture loads for the as-welded compositions are significantly higher than those for the re-heated material. This is as would be expected since during the multi-run welding procedure the material is subjected to a thermal cycle which causes the metal to expand at the same time as its yield stress is reduced. Since the material is under physical restraint this sets up stresses in the material and induces strain.

These repeated thermo-mechanical cycles cause strain ageing of the re-heated weld metal pinning dislocations and raising the yield strength. Residual stresses also act to raise the yield strength. A further result of this strain ageing is that no Lüders strains are observed during low temperature testing. The microstructures of these materials, which are after all commercial electrodes designed for high toughness in the as welded condition, also promote a high yield strength.



The object of the heat treatment carried out on the experimental electrodes was to ensure that these factors did not obscure the effects of alloying on the cleavage behaviour.

5.5 Effect of alloying on general yield strength

Although this area was discussed in section 5.1 in connection with the possible effect of grain size on general yield strength it was clear that the grain size effect did not provide a complete explanation. It was also noted that the change in composition from sample to sample would also affect the constants in the relationship.

It was noted in work on the effects of grain size at constant composition that the lattice friction stress σ_0 had a negative value which was because of the increasing importance of dislocation related effects with decreasing grain size. The materials examined in this research had small grain sizes due to the austenitising heat treatment, grain boundary pinning by inclusions and the presence of large numbers of inclusions to act as ferrite nucleation sites. The effect of alloying on the slip characteristics of the material should therefore be an important factor in the determining of yield strength.

It is known that manganese can modify the deformation characteristics of ferrite (57) as well as affecting cross slip and the length of dislocation pile-ups at grain boundaries (55,58). Nickel in solution produces centres of strain which can

prevent dislocation locking by trapping interstitials such as carbon and nitrogen. Nickel also increases the stacking fault energy and the ability of dislocations to cross slip.

It seems likely, however, that these effects compete with strengthening effects with increasing additions. In the case of the compositions A and E it appears that these levels have been exceeded, A having too much manganese for the nickel content and E having too much nickel for the manganese content.

The effect on composition E appears to be more drastic than that on A but these two compositions 1.6%Mn / 1.5%Ni (E) and 1.0%Mn / 2.5%Ni (A) suggest that the greatest increase in yield strength which will be achieved by alloying effects on the matrix occurs at about 1.0%Mn and 1.5%Ni which corresponds to the composition D.

5.6 Effect of alloying on cleavage fracture strength

As was demonstrated in section 4.5.2.5 the cleavage fracture strengths for the various compositions could be ranked in the order :

D > 7016, 7016C1 > C, G > F > E

The composition A did not show cleavage coincidence with general yielding within the temperature range investigated but was tentatively ranked between C and G.



It can be seen that there is no correlation between this ranking order and that for general yield stress given in section 5.1. This is because the general yield strengths were ranked at a constant temperature of -150°C and although σ_{max} , the cleavage fracture stress is said by Knott to be relatively independent of temperature the general yield strength is not. Only if the coincidence of general yielding with fracture occurred at the same temperature for each composition would we expect this to be the case.

These results demonstrated that both manganese and nickel individually improved the cleavage fracture strength of the material in the range of compositions studied, i.e. up to 1.6% manganese and 2.6% nickel. In combination however it was shown that increasing alloying beyond 1.0% manganese and 1.5% nickel tended to have either no effect (nickel) or a detrimental effect (manganese). This is in agreement with the conclusions in section 5.5 concerning the effect of alloying on general yield strength.

In ferritic steels cleavage proceeds in two stages, firstly cleavage crack initiation and then once a critical flaw size has been achieved for the applied stress this crack propagates through the material. Thus alloying may affect either of these two stages and change the cleavage behaviour of the material.

Initiation of cleavage in ferritic steels requires the pile-up of dislocations as the first step. This can be at intersecting slip



planes, grain boundaries or at inclusions. Since the dependence of cleavage strength on carbide size has been demonstrated it is widely accepted that in wrought materials cleavage initiates at brittle grain boundary carbides.

In this re-heated weld metal though it does not appear that grain boundary material alone is the key to cleavage initiation. If this were the case we would expect to see a correlation between grain size and cleavage fracture strength. There appears to be no such correlation in this instance.

Cleavage initiation is more difficult if the applied stress resulting from a dislocation pile-up can be accommodated by plastic flow of the matrix material around brittle particles. The effects of alloying on the slip characteristics of the material are thus of great importance in determining their influence on cleavage strength.

However, it has also been noted that if increasing alloying increases the yield strength without continuing to improve the microstructure then the toughness of the material will decrease as the matrix is less able to accommodate the stresses at brittle particles by plastic flow.

The effects of manganese and nickel on the slip characteristics of the material include:

- 
- Nickel reduces the room temperature yield strength and can also affect the ductility.
 - Manganese raises the room temperature yield strength.
 - Nickel allows increased cross slip of screw dislocations around cracks and flaws in the material.
 - Nickel makes $\langle 100 \rangle$ dislocations less effective as crack nuclei of the type proposed by Cottrell by spreading their shear misfit.
 - Nickel in solution can trap interstitials such as carbon and nitrogen preventing them from assisting in dislocation locking.
 - In the presence of manganese there appears to be an optimum combination for the above.
 - Nickel can act to increase the strain hardening rate of the matrix.

Of these effects it might be expected that those which improve the materials ability to slip will enhance the cleavage strength whereas those that tend to increase its yield strength will be detrimental. If the degree of alloying exceeds that required to give the beneficial effects then, as was observed further alloying will be counter-productive.



It seems unlikely that these phenomena alone could account for the behaviour observed in these experimental electrodes. It is likely therefore that other effects of alloying on the nature of the re-heated material will also play a role.

Other effects of manganese and nickel on the microstructure of the material include the role that alloying can play in determining both the nature and disposition of inclusions and carbides. A fine dispersion of inclusions in the weld metal is known to produce acicular ferrite since these inclusions provide nucleation sites for the acicular ferrite transformation. The presence of acicular ferrite in as-deposited weld metal is one of the aims of the electrode designers since it is known to promote toughness.

In reheated material the size and dispersion of these inclusions not only affect the grain size of the re-heated material but are also likely to affect the cleavage process. These inclusions will tend to be manganese alumino-silicates as well as other alumina and silicon rich particles..

Under cleavage conditions larger inclusions are the most likely to initiate cleavage under the effect of dislocation pile ups. Modifications can be made to the de-oxidants in electrode coatings to reduce the size of these inclusions. Since manganese is a weak de-oxidant it is possible that increasing additions of manganese in some way affects the inclusion size.

Another determining factor in cleavage initiation is the size and nature of carbides. Manganese refines the structure of the pearlite present in the re heated material and might thus improve its resistance to cleavage initiation by reducing the carbide film thickness. Nickel also acts to refine pearlite in the re heated region by its action as an austenite stabiliser.

Nickel reduces the diffusivity of carbon in ferrite and in the presence of a carbide former such as manganese the carbides formed may reduce the amount of carbon in solution and reduce grain boundary cohesion. Manganese also prevents the formation of grain boundary carbide networks which if present could drastically reduce the cleavage strength.

There may also be an effect on the cohesion between the ferrite matrix and inclusion particles. This could be important because since cleavage initiation is likely to be at these particles then the cohesion between them and the ferrite matrix will affect the growth of the crack beyond the cracked particle.

Inclusions can also generate dislocations as a result of the stresses induced by thermal cycling. Weatherley (102) demonstrated that the greatest stress generated at the interface of a spherical inclusion during cooling is given by the equation:

$$\sigma_{\max} = \left[\frac{6K^2\mu(T_1 - T_2)}{2K^I + K} \right] [\alpha - \alpha^I]$$

Where K^i & K are the bulk moduli of inclusion and matrix, α^i and α are expansion coefficients and μ is the matrix shear modulus. Weatherley calculated from this that when cooled by 600°C an SiO_2 inclusion would produce a stress of $\mu/6$ which is much greater than the value of $\mu/40$ required to generate dislocations at the interface. These large stress concentrations at the interface of the inclusion with the matrix can therefore affect the ease of dislocation nucleation or de-cohesion of the inclusion/matrix interface.

Grain boundary, and possibly inclusion/ferrite cohesion can also be enhanced by the action of manganese in combination with nitrogen. In solution in the ferrite lattice manganese can exhibit short range order which can attract nitrogen. Since manganese is weakly surface active towards ferrite there is a tendency towards segregation at grain, and possibly inclusion boundaries where it may counteract any detrimental effects of nitrogen on cohesion.

Manganese can also affect the inclusion chemistry. In increasing amounts it changes the composition of inclusions making them more manganese rich and reduces their number. In the presence of sulphur manganese reduces the effectiveness of inclusions as nucleators for acicular ferrite by producing a layer of MnS on the surface of inclusions. It is thus possible that these modifications to the chemistry of these inclusions can affect the cohesion between them and the ferrite matrix.

If the cohesive strength between the inclusions and the matrix is

enhanced then there is a possibility that the mode of cleavage initiation will change, perhaps to the cracking of brittle grain boundary carbides. Floreen, Hayden and Devine (19) in their work on nickel alloying showed that there was a relationship between the nickel content and the cleavage initiation mode. At higher nickel contents inclusions were the nuclei whereas at lower nickel contents initiation tended to be at the grain boundary.

The inter-relation between slip related factors and changes in the nature of the non-grain-size microstructural effects can be seen to provide some explanation of the effects of alloying on the cleavage behaviour of these materials.

Thus to summarise:

- Both manganese and nickel improve the slip characteristics of the material up to a certain level. However by raising the yield stress there comes a point where further alloying increases the likelihood of cleavage since strains around inclusions can not be accommodated and the particles crack.
- Alloying can affect the size and distribution of inclusions which in turn affects cleavage initiation.
- Manganese in particular acts to increase the cohesion of grain boundaries and it is suggested that this may also be the case for boundaries between the matrix and inclusion particles. If this



is so it will become more difficult for a crack to propagate from a cracked particle into the matrix.

- One way in which manganese can improve cohesion is by altering the chemistry of the inclusion.

- If the cohesion between the ferrite and the inclusion is sufficiently increased then other initiation sites may come into play. In the examination of fracture surfaces by electron microscopy there was evidence of two regimes. In some cases inclusions had been displaced by the fracture leaving a hole whereas in others undamaged inclusions were still clearly visible in the centre of cleavage facets. Although it appeared clear in most cases that cleavage initiation was at inclusion sites there is obviously more information to be gained from a deeper investigation of the cohesion between the matrix and inclusions as well as the role this plays in fracture.

- There appears to be an optimum composition of 1.0% manganese and 1.5% nickel for the greatest improvement in cleavage fracture strength as a result of the interaction of these factors.

5.7 Correlation between K_{IC} and cleavage fracture strength

Although it became clear in the previous section that the process of initiation was of the greatest importance in determining the magnitude of the cleavage fracture strength it might be expected that the energy required for cleavage crack propagation would

play a role in determining the material's fracture toughness. One observation which might be of value in determining whether this is indeed the case could be the density of river markings on the fracture surface. If these markings show a large degree of branching this would indicate that cleavage cracks had difficulty in propagating and so changed to more favourable fracture paths.

The ranking orders for K_{Ic} and cleavage fracture strength show a considerable degree of correspondence as can be seen below:

K_{Ic} D > 7016 > F > 7016C1 > C > A > (E)

σ_{max} D > 7016, 7016C1 > C , (A) , G > F > E

Disregarding the compositions where no valid result is available for these parameters the only composition which shows an unusual result is electrode F which showed better fracture toughness than might be expected if cleavage fracture strength was directly related to fracture toughness. Reference to section 4.6.3 shows that F showed numerous river markings on the fracture surface suggesting that an improved resistance to cleavage crack propagation might explain this apparent discrepancy. An alternative explanation might be that the temperature at which coincidence of fracture with general yielding occurred was higher for this composition than for the other samples giving a valid K_{Ic} value. Coincidence occurred at -150°C whereas the other values for cleavage fracture stress are based on the -170°C test. This

suggests that for this family of alloys there may in fact be some temperature dependence of the cleavage fracture strength which is significant.

Otherwise the similarity between the results for these two parameters suggest that in re-heated material, where the effects of alloying on the microstructure of the as-welded material are to a large extent eliminated plane strain fracture toughness tends to be governed by similar mechanisms to those which determine the cleavage behaviour

5.7 Conclusions and suggestions for further research

The aim of this research was to investigate the effects of manganese and nickel on the cleavage behaviour of ferritic weld metal and in so doing to suggest possible mechanisms for the results found by previous workers. The findings of this research can be summarised as follows:

- The grain size effect is at least an important contributor to the variation in yield strength from composition to composition but is not in itself the complete explanation.
- Grain size is affected by the microstructure of the as-deposited material since inclusions pin the austenite grain boundaries on re-heating.
- Grain sizes after heat treatment depend on an interplay between the effects of alloying on transformation temperatures, the



grain sizes and phases present in the as-deposited weld metal and the distribution of inclusions.

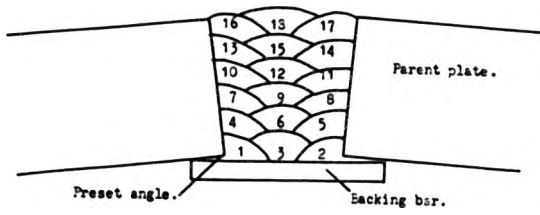
- The effect of alloying on the slip characteristics of the material is a factor in determining the yield strength.
- Yield strength did not continue to increase with increasing alloying additions beyond about 1.0%Mn and 1.5%Ni.
- Manganese and nickel individually improved the cleavage fracture strength of the material but in combination increasing alloying beyond 1.0% manganese and 1.5% nickel had a detrimental effect.
- This optimum level is the result of an inter-action between the effects of alloying on: slip characteristics ,yield stress, the size and distribution of inclusions ,the cohesion of grain boundaries and the cohesion of boundaries between the matrix and inclusion particles.
- Manganese can improve cohesion by altering the chemistry of the inclusion.
- In the examination of fracture surfaces by electron microscopy there was evidence of variation in the cohesion between samples. In some cases inclusions had been displaced by the fracture leaving a hole whereas in others undamaged inclusions were still clearly visible in the centre of cleavage facets.

- 
- A composition of 1.0% manganese and 1.5% nickel gives the best cleavage properties.
 - In re-heated material plane strain fracture toughness is influenced by similar factors to those which determine the cleavage behaviour.

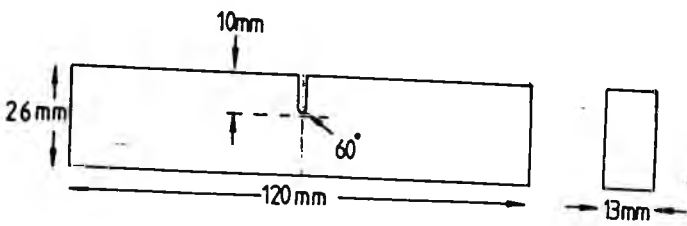
These findings help to explain the previously observed effects of manganese and nickel on cleavage as well as revealing new insights into their action and showing correlations with other material parameters thus fulfilling the original aims of the research. The role of these alloying additions in determining the nature and cohesion of inclusions and the effect of this on the cleavage behaviour of the material is worthy of further investigation.



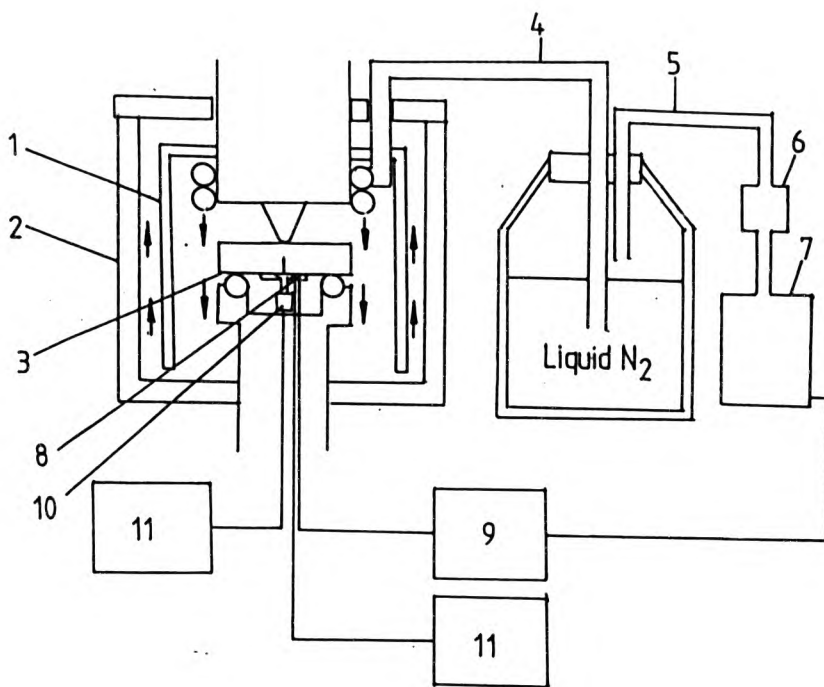
FIGURES



Fig(3.3.1) The position and sequence of welding runs and test plate clamping arrangement.

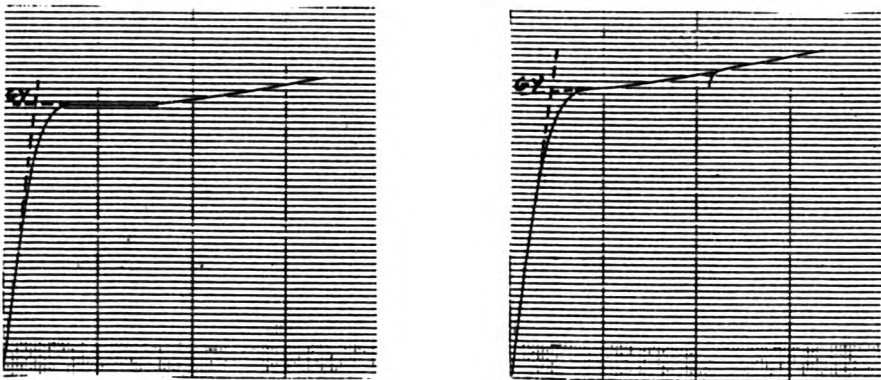


Fig(3.4.1) Test piece geometry

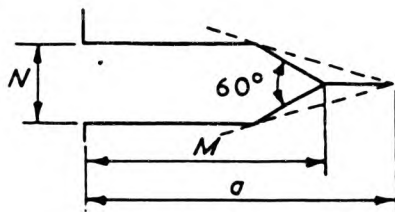


- | | |
|-----------------------------|-------------------------|
| 1 - Inner Chamber | 7 - Compressor |
| 2 - Outer Insulated Chamber | 8 - Thermocouples |
| 3 - Test-piece | 9 - Temperature Control |
| 4 - Liquid Nitrogen Line | 10 - Clip Gauge |
| 5 - Compressed Air Line | 11 - Chart Recorders |
| 6 - Air Dryer | |

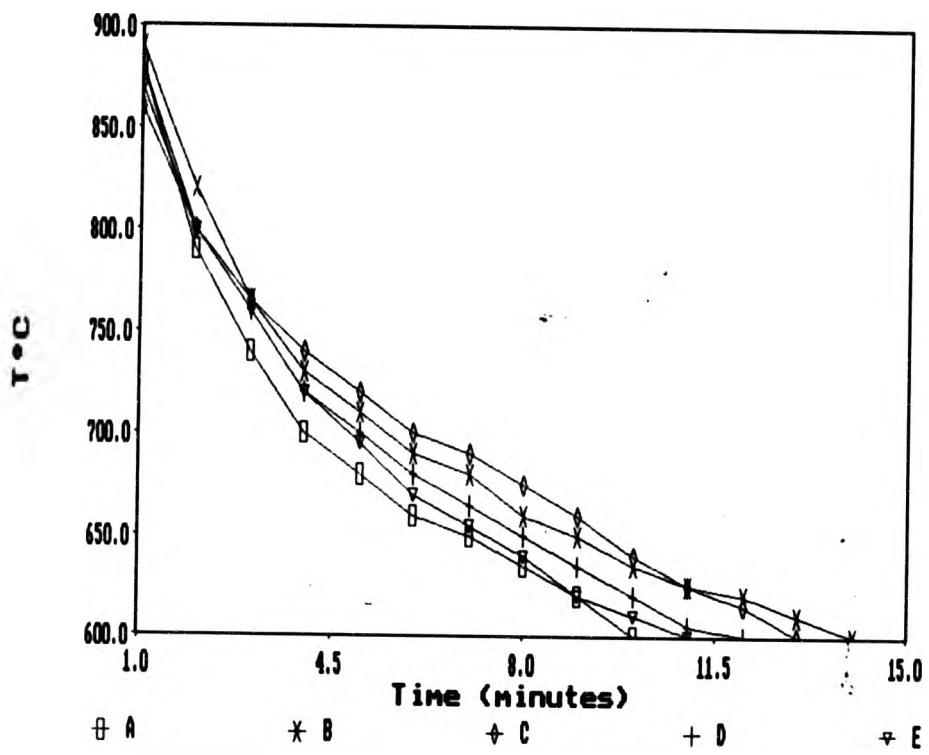
Fig(3.6.1) Cryostatic test cell



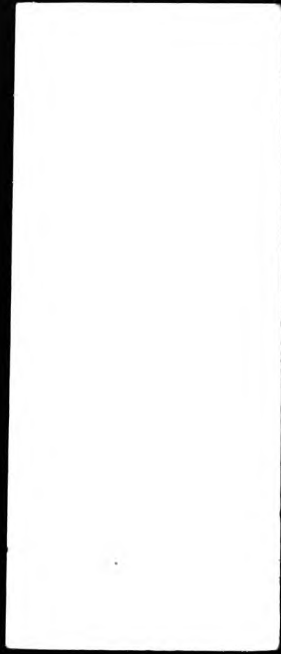
Fig(3.7.5.1) Geometric construction to obtain general yield load



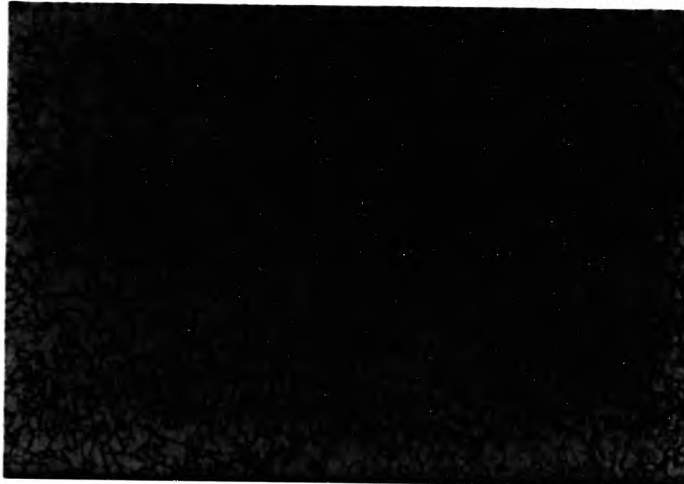
Fig(3.8.1.1) Limiting envelope in which the fatigue pre-crack for K_{Ic} test-piece must fall



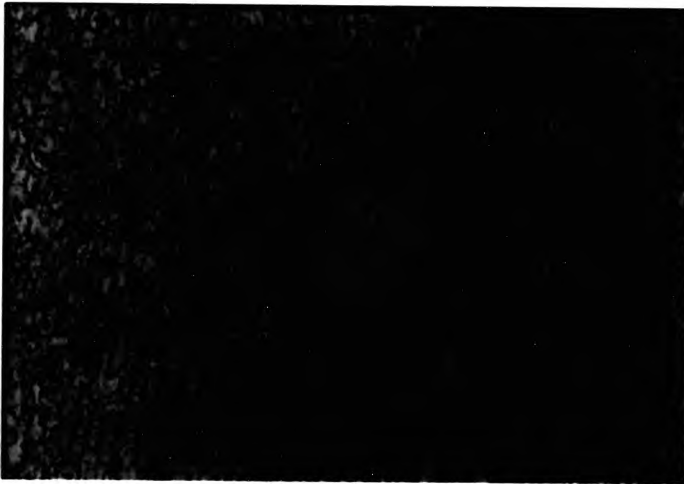
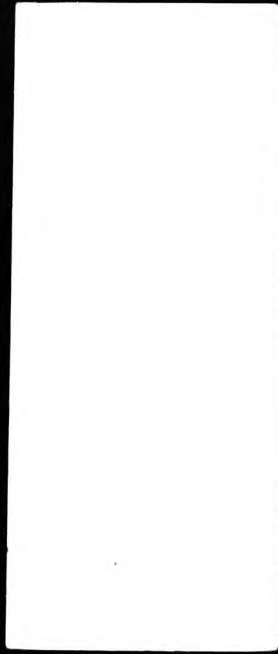
Fig(4.2.1) Typical cooling curves after heat treatment
 (example shown is for composition A)



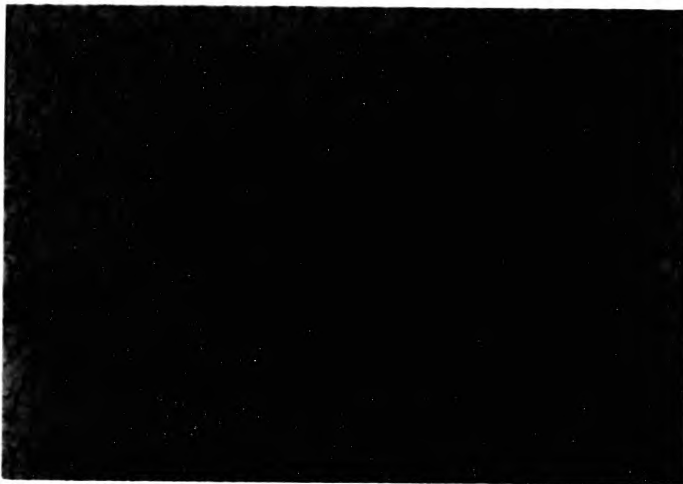
Fig(4.3.1) Photo-micrograph of re-heated microstructure 7016



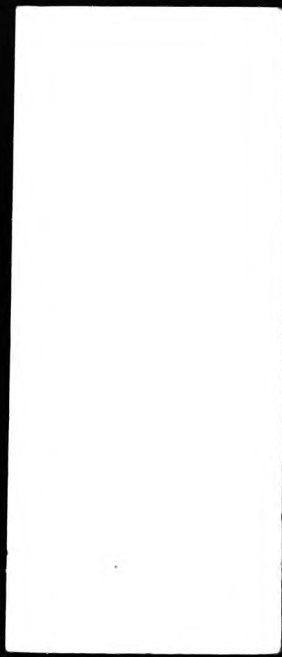
Fig(4.3.2) Photo-micrograph of re-heated microstructure 7016C1
(x 150)



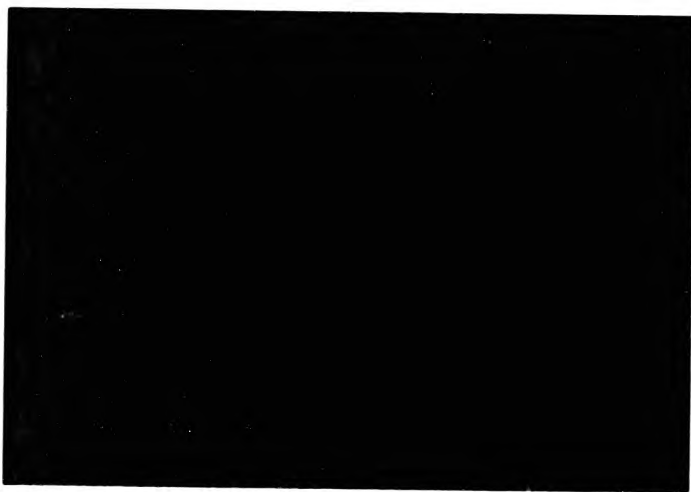
Fig(4.3.3) Photo-micrograph of re-heated microstructure A



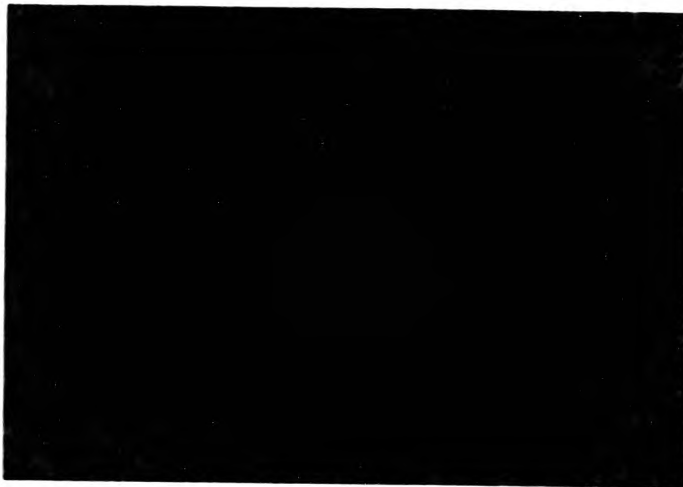
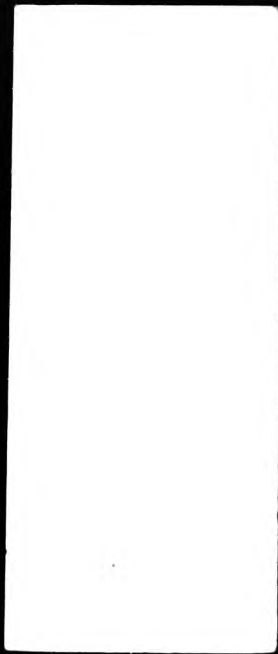
Fig(4.3.4) Photo-micrograph of re-heated microstructure C
(x 150)



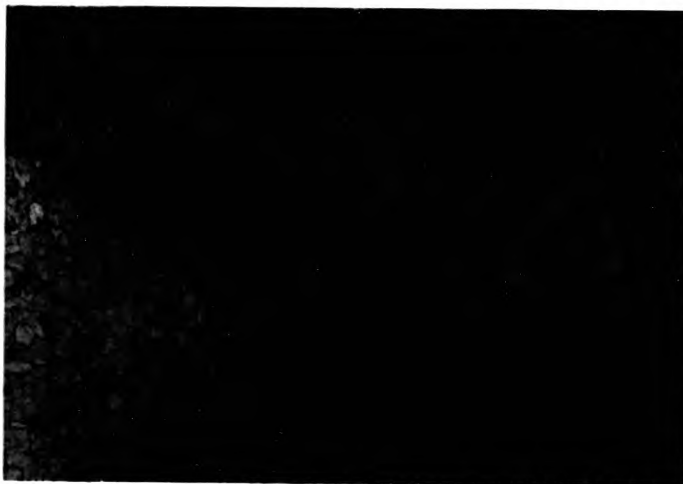
Fig(4.3.5) Photo-micrograph of re-heated microstructure D
(x 150)



Fig(4.3.6) Photo-micrograph of re-heated microstructure E
(x 150)

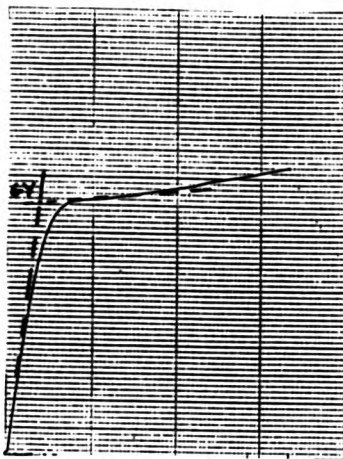


Fig(4.3.7) Photo-micrograph of re-heated microstructure F

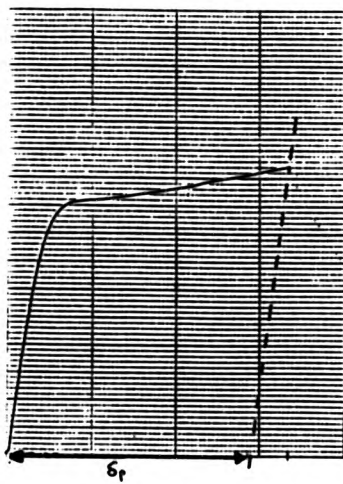


Fig(4.3.8) Photo-micrograph of re-heated microstructure G

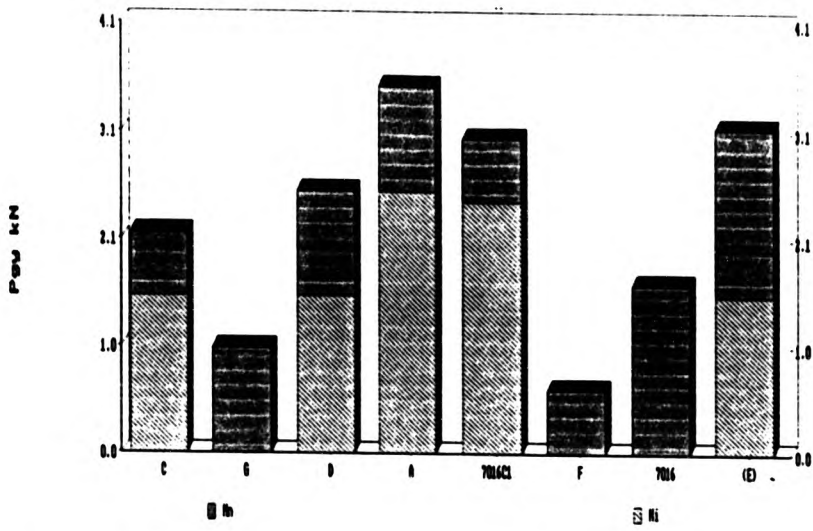
(x 150)



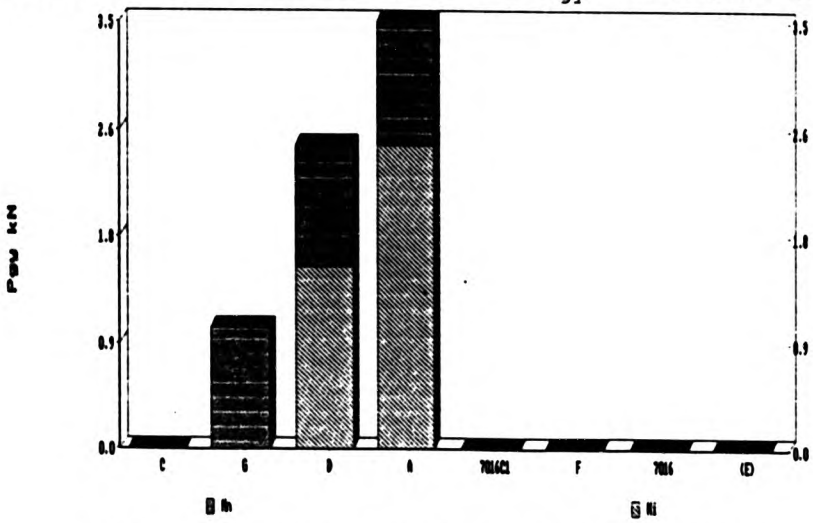
Fig(4.5.1.1) Typical form of load versus clip gauge opening curve



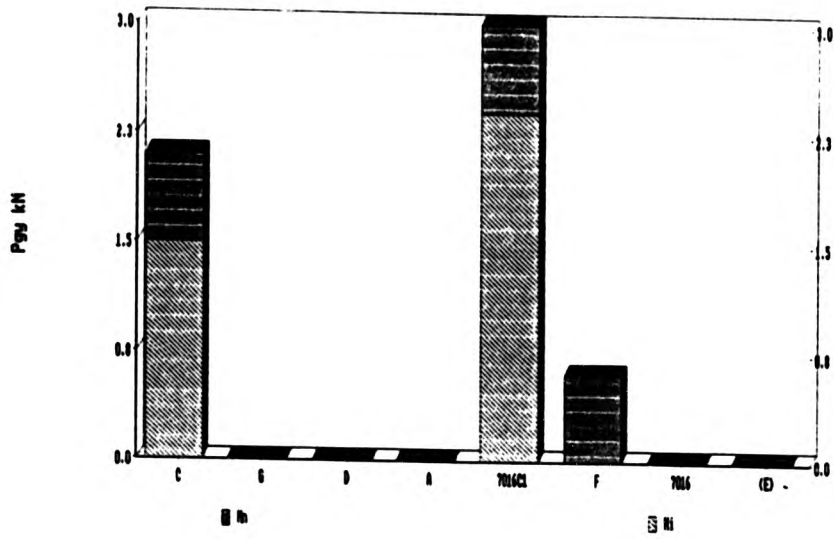
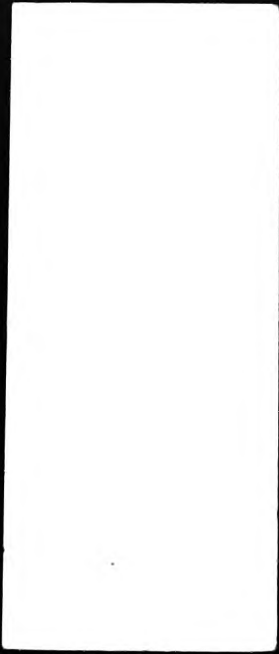
Fig(4.5.1.2) Offset method to determine amount of plastic deformation



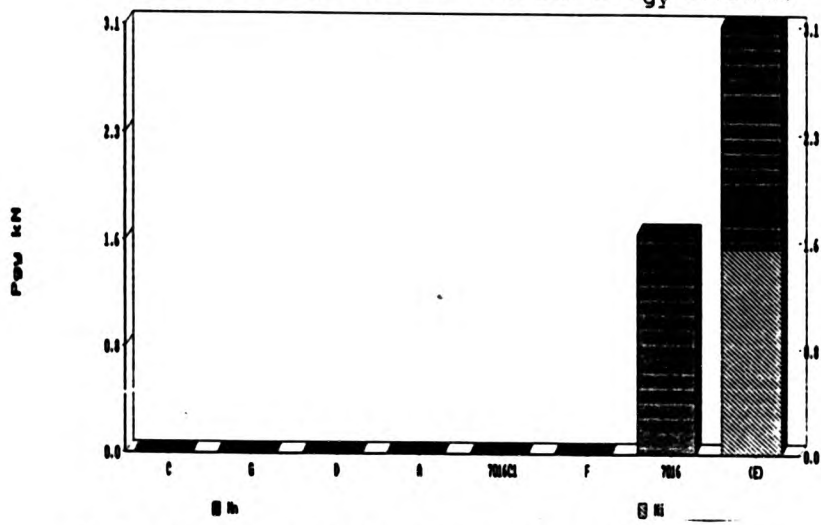
Fig(4.5.2.3.1) Mn% and Ni% in order of P_{gy} (all compositions)



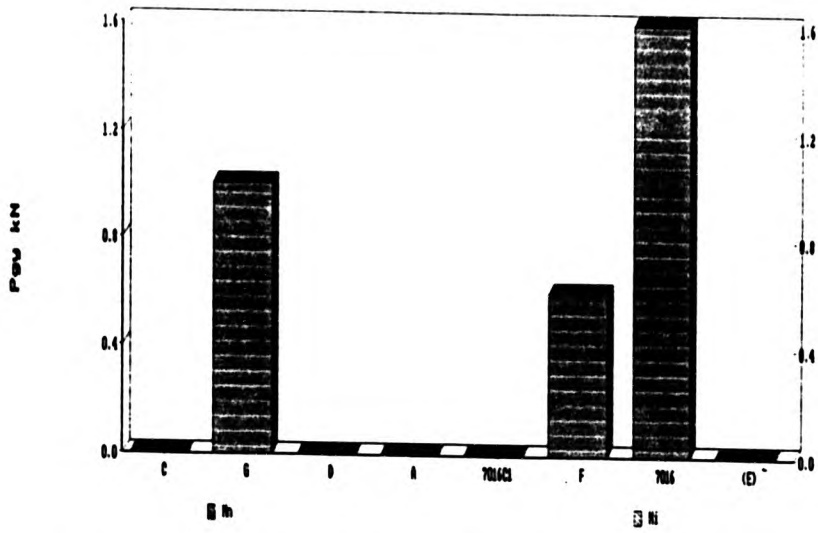
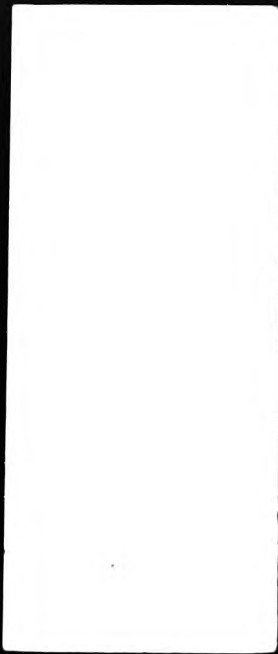
Fig(4.5.2.3.2) Mn% and Ni% in order of P_{gy} (1%Mn)



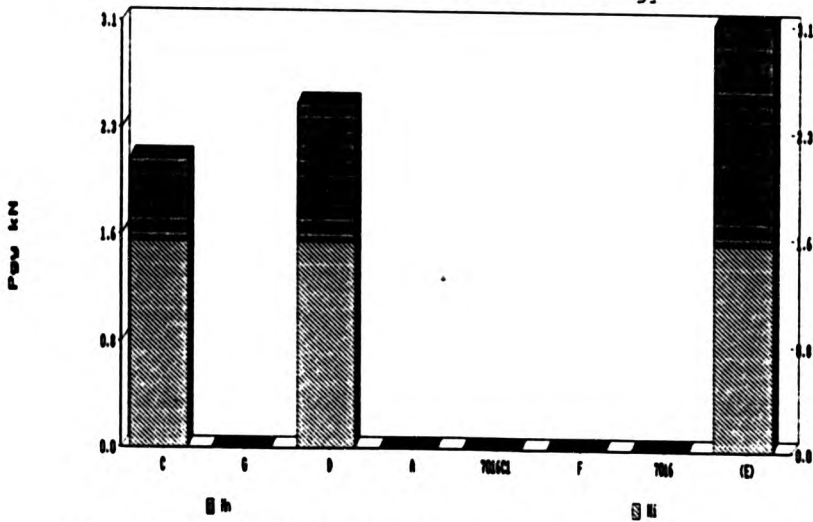
Fig(4.5.2.3.3) Mn% and Ni% in order of Pgy (0.6%Mn)



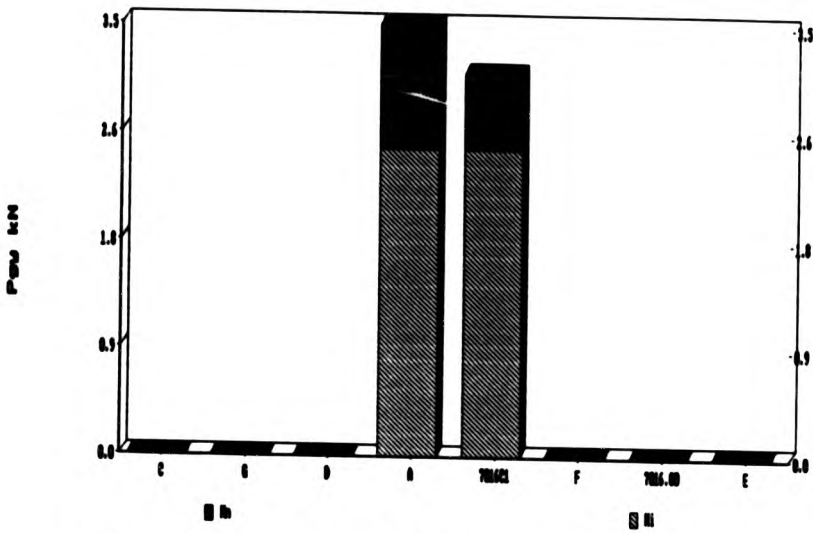
Fig(4.5.2.3.4) Mn% and Ni% in order of Pgy (1.6%Mn)



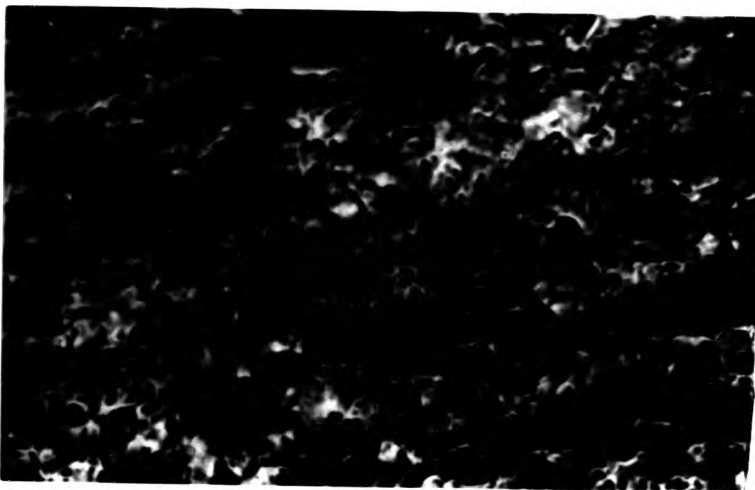
Fig(4.5.2.3.5) Mn% and Ni% in order of P_{gy} (0.0%Ni)



Fig(4.5.2.3.6) Mn% and Ni% in order of P_{gy} (1.5%Ni)



Fig(4.5.2.3.7) Mn% and Ni% in order of P_{gy} (2.5%Ni)



Fig(4.6.1.1) Scanning electron micrograph of -105°C fracture surface sample as-welded 7016 (x 2000)

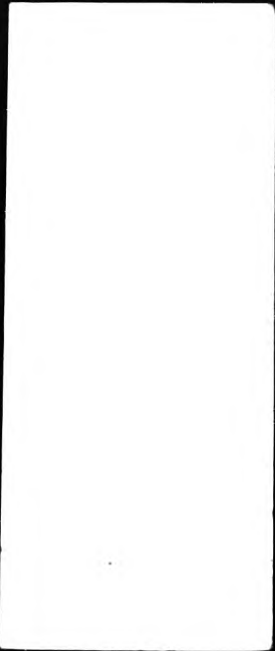
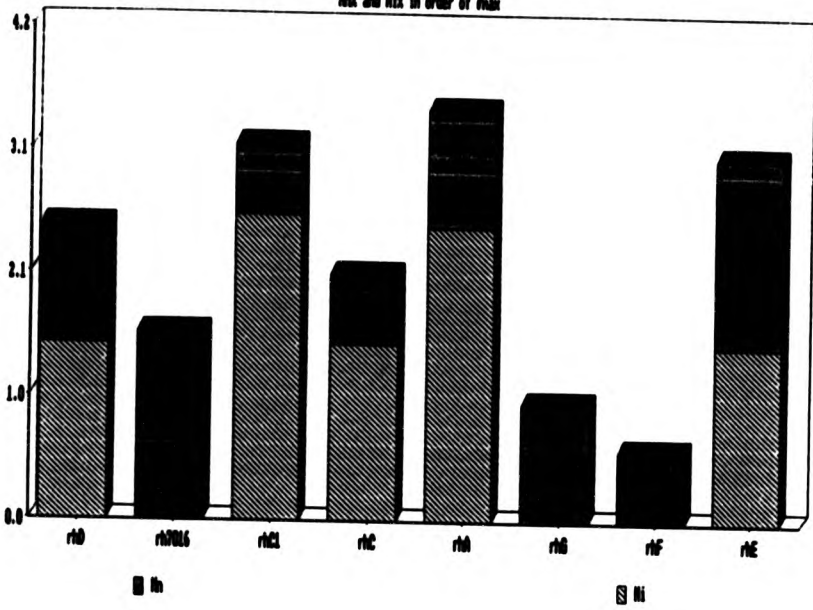


Fig 4.5.2.5.1
Rix and Rix in order of max





Fig(4.6.1.2) Scanning electron micrograph of -105°C fracture surface sample as-welded 7016 (x 2000)



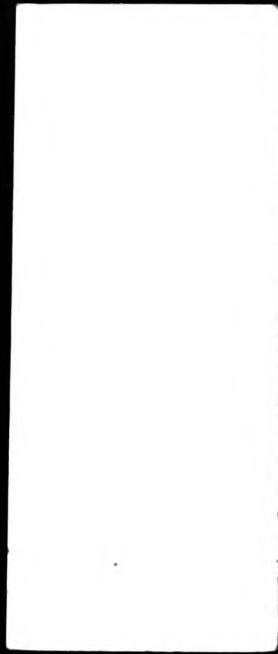
Fig(4.6.1.3) Scanning electron micrograph of -105°C fracture surface sample as-welded 7016 (x 2000)



Fig(4.6.1.4) Scanning electron micrograph of -105°C fracture surface sample as-welded 7016 (x 2000)



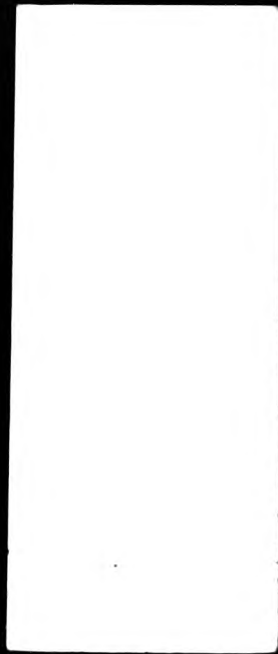
Fig(4.6.1.5) Scanning electron micrograph of -150°C fracture surface sample as-welded 7016 (x 2000)



Fig(4.6.1.6) Scanning electron micrograph of -150°C fracture surface sample as-welded 7016 (x 2000)



Fig(4.6.1.7) Scanning electron micrograph of -150°C fracture surface sample as-welded 7016C1 (x 2000)



**Fig(4.6.2.1) Scanning electron micrograph of -150°C fracture
surface sample re-heated 7016 (x 2000)**



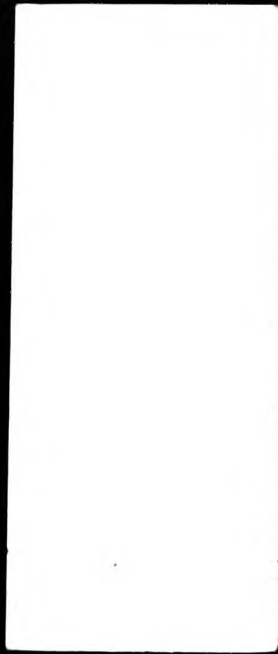
**Fig(4.6.2.2) Scanning electron micrograph of -150°C fracture
surface sample re-heated 7016C1 (x 2000)**



Fig(4.6.3.1) Scanning electron micrograph of -150°C fracture surface sample re-heated A (x 2000)



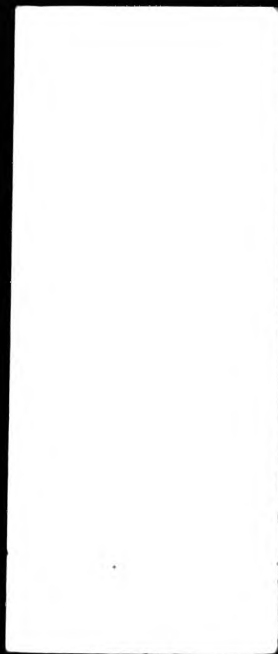
Fig(4.6.3.2) Scanning electron micrograph of -150°C fracture surface sample re-heated C (x 2000)



Fig(4.6.3.3) Scanning electron micrograph of -150°C fracture surface sample re-heated D (x 2000)



Fig(4.6.3.4) Scanning electron micrograph of -150°C fracture surface sample re-heated E (x 2000)



Fig(4.6.3.5) Scanning electron micrograph of -150°C fracture surface sample re-heated F (x 2000)



Fig(4.6.3.6) Scanning electron micrograph of -150°C fracture surface sample re-heated G (x 2000)

**PAGINATION
ERROR**

p 140

LITERATURE CITED

- (1) Rosenthal D, Congres National des science, Comptes Rendus, Bruxelles, 2, 1277, 1935.
- (2) Shinoda T and Doherty J. The Welding Institute, Report No 74/1978/PE 1978.
- (3) Andersson BAB, Journal of Engineering Materials and Technology ASME, 100, p356, 1978.
- (4) Kou S, Metallurgical Transactions, 12A, 1981, p2025.
- (5) Widgery DJ and Saunders GG, Welding Institute Research Bulletin, 16, 10, 1975, pp277-281.
- (7) Abson DJ and Dolby RE, Welding Institute Research Bulletin, July 1978, pp202-207.
- (8) Widgery DJ, Welding Research International, 5, 2, 1975, p1.
- (9) Widgery DJ, Welding Journal, 55, 3, 1976, p57s.
- (10) Abson DJ and Dolby RE, Welding Institute Research Bulletin, April 1980, pp100-103.
- (11) Jenkins M, Stevens SM, Welding Institute Research Bulletin, Jan 1977, p3.
- (12) Hopkins and Tipler, JISI, 177, 1954, p110.
- (13) Abson DJ, Dolby RE and Hart PHM, Welding Institute Members Report, 67/1978/M, 1978.
- (14) Evans GM, Welding Journal, 59, 3, 1980, p67.
- (15) Evans GM, IIW Doc IIA -432-77, 1977.
- (16) Evans GM, IIW Doc IIA -529-81, 1981.
- (17) Evans GM, IIW Doc IIA -460-78, 1978.
- (18) Evans GM, IIW Doc IIA -490-79, 1979.
- (19) Taylor DS and Evans GM, 2nd International Conference on Offshore Welded Structures, The Welding Institute, 1983, paper

29.

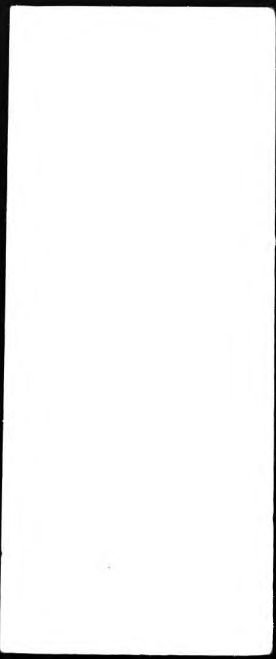
- (20) Cottrell AH, Trans AIME, 212, p192, 1958.
- (21) McMahon CJ and Cohen M, Acta Metallurgica, 13, p591, 1965.
- (22) Smith E, Proc Conf Physical Basis of Yield and Fracture, Oxford Inst of Phys and Phys Soc, London, 1969, p36.
- (23) Almond E, Timbres DH and Embury JD, Proc 2nd Int Conf Fracture, Brighton, Chapman and Hall, London, 1969, p253.
- (24) Abson DJ and Pargeter RJ, Welding Institute Contract Report for BOC Murex, May 1980.
- (25) Choi CL and Hill DC, Welding Journal, 57, 8, 1978, pp232-236.
- (26) Harrison PL and Farrar RA, Journal of Materials Science, 16, 1981, pp2218-2226.
- (27) Cochrane RC, Trends in Steels and Consumables for Welding, The Welding Institute, 1979, pp661-673.
- (28) Barritte GS and Edmonds DV, Advances in the Physical Metallurgy and Applications of Steels.
- (29) Barritte GS, Ricks RA and Howell PR, Strength of Metals and Alloys (ICSMA6), (ed Griffiths RC) Pergamon, Oxford, 1983, pp121-126.
- (30) Garland JG and Kirkwood PR, Welding & Metal Fabrication, 44, 3, 1976, pp217-224.
- (31) Tuliani SS, Boniszewski T and Eaton NF, Welding & Metal Fabrication, 40, 1972, pp247-259.
- (32) Ricks RA, Howell PR and Barritte GS, Journal of Material Science, 17, 1982, pp732-740.
- (33) Ricks RA, Barritte GS and Howell PR, Proc Int Conf Solid State Phase Transformations, Pittsburgh, August 1981, National Science

- Foundation and Metallurgical Society of AIME, pp463-468.
- (34) Pargeter RJ, Welding Institute Research Bulletin, 24, 7, 1983, pp215-220.
- (35) Devillers L et al, The Effects Of Residual Impurity and Microalloying Elements on Weldability and Weld Properties, Paper 1, The Welding Institute, 1984.
- (36) Sakuma T and Honeycombe RWK, Materials Science and Technology, May 1985, p351.
- (37) Taylor DS and Evans GM, Metal Construction, 15, 8, 1983, pp438-443.
- (38) Pickering FB, Microalloying '75, Union Carbide Corporation, New York, 1977, pp9-30.
- (39) Sakaki H, Journal Japanese Welding Society, 29, 6, 1960, pp474-484.
- (40) Evans GM, Welding Review, 1, 1, 1982, pp14-20.
- (41) Bosward IG and John R, Trends in Steels and Consumables for Welding, The Welding Institute, 1979, pp135-150.
- (42) Dorsch KE and Stout RD, Welding Journal, 40, 3, 1961, pp97s-105s.
- (43) Tremlett HF, Baker RG and Wheatley JM, British Welding Journal, 8, 1961, pp437-454.
- (44) Dolby RE, Research Report 14/1976/M, The Welding Institute, 1976
- (45) Dolby RE, Fracture '79, (ed Garrett GG and Marriott DL) Pergamon, Oxford, 1979, pp117-134.
- (46) Garstone J and Johnson FA, British Welding Journal, 10, 5, 1963, pp224-230.
- (47) King G, Jarman RA and Judson P, (unpublished)

- 
- (48) Widgery DJ, Research Report M/27/68, British Welding Research Association, Abington, 1968.
- (49) Evans GM, Welding Journal, 61, 4, 1982, pp125s-132s.
- (50) Evans GM, IIW Doc II-A-666-86, 1986.
- (51) Evans GM, Oerlikon Schweissmitteilung, 40, 99, 1982, pp17-31.
- (52) Abson DJ, Research Report 194/1982, The Welding Institute, Abington, 1982.
- (53) Taylor DS, Welding & Metal Fabrication, 50, 9, 1982, pp452-460.
- (54) Morigaki O, IIW Doc II-955-81, 1981.
- (55) Stoloff NS, Fundamental Phenomena in Materials Science, 4, 1967, p197.
- (56) Pacey AJ and Kerr HW, Welding & Metal Fabrication, November 1978, p613.
- (57) Jolley W and Kottcamp EM, Trans ASM, 59, 1966, p439.
- (58) Honeycombe RWK, Steels: Microstructure and Properties, EA Arnold, 1981.
- (59) Ohwa T, IIW Doc II-221-62, 1962.
- (60) Mentink H, Scandinavian Offshore Symposium, Philips, Eindhoven, 1983.
- (61) Morigaki O et al, IIW Doc II-746-75, 1975.
- (62) Nutting J, JISI Centenary Meeting, 1969, p123.
- (63) Lesley WC, Physical Metallurgy of Steels, McGraw-Hill, 1981.
- (64) Judson P and McKeown D, Offshore Welded Structures, Paper 3, The Welding Institute, Abington, 1983.
- (65) Pechennikov VI et al, Weld Prod, 26, 10, 1979, pp52-53.
- (66) Hirabayashi K et al, Physical Metallurgy of Weldments, Niagara Falls NY, Metallurgical Society Of AIME, 1976.

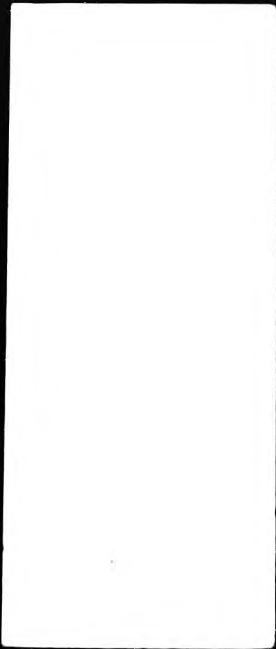
- 
- (67) Towers OL, *Metal Construction*, 18, 3, 1979, pp171R-176R.
- (68) Wilshaw TR and Pratt PL, *Proc Int Conf Fracture, Sendai, Japan, 1965*, pp973-991.
- (69) Neumann A, Benois FF and Hilbert K, *Schweisstechnik*, 18, 9, 1968, pp385-390.
- (70) Rosenfield AR and Shetty DK, *Elastic Plastic Fracture Test Methods: The Users' Experience*, ASTM STP 856 (ed Wessel ET and Loss FJ) ASTM, 1985, pp196-209.
- (71) Almond EA and Embury JD, *Metal Science Journal*, 2, 1968, p194.
- (72) Sandstrom R and Bergstrom Y, *Metal Science*, 18, 1984, p177.
- (73) Knott JF, *Fundamentals of Fracture Mechanics*, Butterworths, 1973.
- (74) Honeycombe RWK, *The Plastic Deformation of Metals*, Edward Arnold, London, 1968.
- (75) Norstrom LA and Vingsbo O, *Metal Science*, 13, 1979, p677.
- (76) Ritchie RO, Francis B and Server WL, *Metallurgical Transactions*, 7A, 1976, p831.
- (77) Eshelby JD, *Solid State Physics*, (eds Seitz F and Thurnbull D), 3, 1956, pp79-141.
- (78) Rice JR, *Journal Applied Mechanics*, 35, 1968, pp379-386.
- (79) Rice JR, *Fracture: An Advanced Treatise*, (ed Liebowitz H), 2, Academic Press, New York, 1968, pp191-311.
- (80) Kameda J and McMahon CJ, *Metallurgical Transactions*, 11A, 1980, p91.
- (81) Kotilainen H, *Fracture Mechanics: Twelfth Conference*, ASTM SPT 700, ASTM, 1980, pp352-367.
- (82) Yaroshevich VD and Ryvinka DG, *Soviet Physics - Solid State*, 12, 2, 1970, pp363-370.

- 
- (83) Green AP and Hundy BB, *Journal Mech Phys Solids*, 4 (II) 1956, p128.
- (84) Hauser FE et al , *Trans AIME*, 206, 1956, p589.
- (85) Griffiths JR and Owen DRJ, *Journal Mech Phys Solids*, 19, 1971, p419.
- (86) McMahon CJ and Cohen M, *Acta Metallurgical*, 13, 1965, p591.
- (87) Hodgson DE and Tetelman AS, *Fracture 1969*, (ed Pratt PL), Chapman and Hall, London, 1969, p260.
- (88) Curry DA and Knott JF, *Metal Science*, 12, 1978, p511.
- (89) Curry DA , *Metal Science*, 18, 1984.
- (90) Stroh AN , *Proceedings Royal Society*, A223, 1954, p404.
- (91) Ritchie RO, Knott JF and Rice JR, *Journal Mech Phys Solids*, 21, 1973, p395.
- (92) Malkin J and Tetelman AS, *Engineering Fracture Mechanics*, 3, 2, 1971, pp151-167.
- (93) Floreen S , Hayden HW and Devine TM, *Metallurgical Transactions*, 2, 1971, p1403.
- (94) McRobie DE and Knott JF, *Materials Science and Technology*, 1, 1985, p360.
- (95) Tweed JH and Knott JF, *Metal Science*, 17, 1983, pp45-54.
- (96) Edwards BC, Whapham AD and Popkiss EW, *Contract Report for BOC Murex*, AERE Harwell, December 1979.
- (97) Tweed JH, *Progress Report to BOC Murex*, November 1980.
- (98) Atkins M, *Atlas of CCT diagrams for engineering steels*, BSC.
- (99) Weichert R and Schonert K, *Journal Mech Phys Solids*, 24, 1974, p127.
- (100) Knott JF, *JISI*, 204, 1966, p104.



(101) King G, PhD transfer report,1982.

(102) Weatherley GC,Metal Science Int,2,1968,p237.



THE BRITISH LIBRARY DOCUMENT SUPPLY CENTRE

TITLE THE EFFECT OF MANGANESE AND NICKEL ON THE CLEAVAGE FRACTURE
STRENGTH OF FERRITIC WELD METAL

AUTHOR Andrew Robert Brian Sandford

INSTITUTION and DATE City of London Polytechnic 1990
C.H.A.A.

Attention is drawn to the fact that the copyright of this thesis rests with its author.

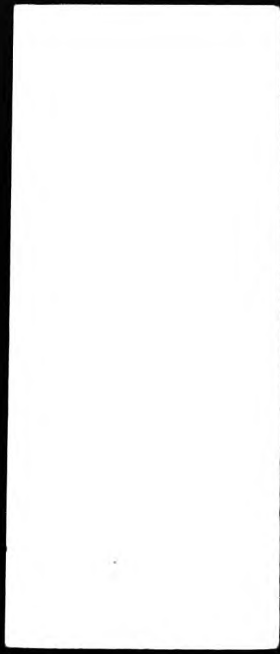
This copy of the thesis has been supplied on condition that anyone who consults it is understood to recognise that its copyright rests with its author and that no information derived from it may be published without the author's prior written consent.

1	2	3	4	5	6	8
cms.						

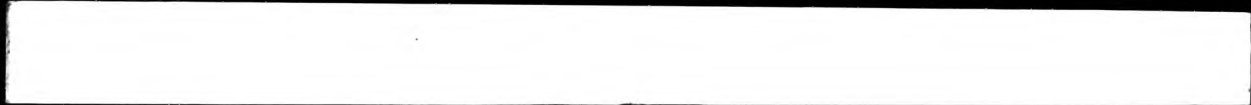
THE BRITISH LIBRARY
DOCUMENT SUPPLY CENTRE
Boston Spa, Wetherby
West Yorkshire
United Kingdom

REDUCTION X 20

C.H.A.A. 5



DX



9	4	4	6	3
----------	----------	----------	----------	----------

